Assignment of Si—O vibrational modes in the IR spectra of C-S-H phases based on single-crystal polarized IR and Raman spectra of 14 Å tobermorite, jennite, and jaffeite

Krassimir Garbev [a,*], Biliana Gasharova [b], Angela Ullrich [a], Günter Beuchle [a], Peter Stemmermann [a]

[a] Institute for Technical Chemistry (ITC), Karlsruhe Institute of Technology, Karlsruhe 76344, Germany
[b] Institute for Beam Physics and Technology (IBPT), Karlsruhe Institute of Technology, Karlsruhe 76344, Germany

Keywords:
C-S-H
IR spectra
14 Å tobermorite
Jennite
Jaffeite

A B S T R A C T

This article explains the vibrational modes in the Si—O stretching range in the IR spectra of synthetic C-S-H phases with varying C/S ratios. These are compared with selected *in situ* spectra of hydrates of OPC, and those of synthetic crystalline hydrates. The assignments were supported by ^{29}Si NMR and trimethylsilylation (TMS) data. IR and Raman polarized spectra of oriented crystals of 14 Å tobermorite, jennite and jaffeite enabled direct observation of the Si—O vibrational modes. They were successfully resolved based on the involvement of specific silicon (paired, bridging) and oxygen (bridging, non-bridging) atoms, and were compared with existing theoretical data. The resemblance between the IR spectra of synthetic C-S-H and those formed upon hydration of OPC, proves the suitability of model C-S-H phases for understanding hydration processes. Some uncertainties in the assignment of the C-S-H bands observed in existing *in situ* IR experiments are discussed, and potential sources of error identified.

1. Introduction

The investigation of the hydration mechanisms of Ordinary Portland Cement (OPC) has been a primary topic for cement chemists for more than a century. Various theories have been developed to explain the process of cement hydration [1]. A strong correlation between dissolution, saturation, nucleation, and growth has been found, highlighting a close linkage to the field of aqueous solution thermodynamics [2].

One of the biggest analytical challenges is the observation and especially the quantification of hydration reactions at the very beginning of the process. Although recent developments in XRD methods provide relatively quick measurements, it is still challenging to obtain powder patterns in a 2Θ range reasonable for Rietveld analysis in a very short time using standard equipment. Additionally, the detectability of certain hydration phases depends on their critical crystal size, which hampers the detection of nuclei at the very early stages of formation. Overlapping reflections, small crystal size, and intrinsic disorder prevent the detection of C-S-H phases even at later stages of hydration. Several other methods have been utilized for *in situ* monitoring of cement hydration, such as Raman spectroscopy [3], demonstrating the power of vibrational spectroscopy as a tool for observation of intermediate products at early stages. However, several limitations of Raman spectroscopy could influence the results. These include possible fluorescence, the local nature of sampling, changes due to laser power and the long acquisition times needed to obtain reasonable spectra of nanocrystalline C-S-H phases.

Attenuated total reflection infrared (ATR-IR) spectroscopy, being independent of long-range structural ordering, provides a powerful tool for directly monitoring the formation and growth of C-S-H. Another advantage of this method is the ability to obtain complete spectra in the mid- infrared range within seconds. Its high sensitivity to different H_2O environments allows for quick estimation of water consumption, nucleation and growth of hydrate phases during the very early stages of cement hydration. ATR-IR has proven to be a reliable method for quantification based on multivariate calibration [4,5], making it possible to obtain quantitative information from *in situ* hydration experiments, although it requires considerable effort.

ATR-IR spectroscopy provides not only information on the evolution

* Corresponding author.
E-mail address: krassimir.garbev@kit.edu (K. Garbev).

of phase contents, but also on the structural development of phases during hydration. In particular, the changing silicate structure in the low-crystalline C-S-H phase is extensively discussed in the literature. The existence of more than one C-S-H phase was proven as early as 1950 [6], followed by the determination of the variation of C/S-ratio with hydration progress in 1962 [7].

In situ ATR-IR has been applied in several studies on cementitious systems [8–10]. In a previous study by Ylmen et al. [8], *in situ* ATR data was validated by *ex situ* data on freeze-dried samples by subtracting the water background from the *in situ* spectra. Additionally, the evolution of the Si—O stretching mode of C-S-H was compared to calorimetric data by subtraction of an initial spectrum acquired after 2 min. This approach was also pursued by Higl et al. [9] who developed a semi-quantitative analysis of C-S-H formation from C_3S by taking NMR data into account. They developed a complex peak fitting strategy that included subtraction of the water signal, linear background correction, and the creation of difference spectra by subtracting the initial spectrum. Another study by John and Stephan [10] includes fits to the characteristic modes of different silicate units. However, the former focuses on pure alite, while the latter examines a mixture of portlandite and colloidal nano-silica suspension.

The motivation for our present study is triggered by three major issues identified in previous investigations. First and foremost, no extended research applying *in situ* IR on more complex cement systems has been conducted so far. Secondly, there is still inconsistency in the attribution and interpretation of individual Si—O bands, which might not be obvious to non-specialists in vibrational spectroscopy. Since the pioneering work of Yu et al. [11], subsequent studies have mostly used their assignment without delving further into details. Due to the expected change of the polymerization degree of the silicate units in C-S-H phases with varying C/S ratio, it is common to refer to the IR bands as modes of specific units in terms of Q^0, Q^1, Q^3, similarly to the interpretation of ^{29}Si NMR signals. While this approach is suitable for NMR and Raman data, the intrinsic broadness of the IR bands makes it less obvious in IR spectra. There has been no attempt to differentiate between contributions from vibrations involving Si-non-bridging oxygens (O_{nbr}) and Si-bridging oxygens (O_{br}). Additionally, using assignments based on calculations of IR spectra for crystalline model materials such as 14 Å tobermorite and jennite [12] could be helpful but also risky without experimental polarized spectra, as we will show later. Third reason is the different and rather complex evaluation of the development of IR bands upon hydration, which can lead to possible misinterpretation. For example, in the work of Ylmen et al. [8], the evolution of the C-S-H band is estimated based on its intensity rather than integral absorption (peak area), resulting in unexpected growth rate outcomes. Using complex subtraction procedures such as those employed by Higl et al. [9] can manipulate the spectra to an extend that leads to incorrect band ratios, thus postulating wrong frequency for the main Si—O band and delivering contradictory assignments.

The primary purpose of this manuscript, which is part of an extended work on *in situ* cement hydration, is to address existing ambiguities in the assignment of IR bands in the high-frequency envelope of the spectra of C-S-H and to extend their interpretation in terms of specific Si-O_{nbr} and Si-O_{br} modes. This will establish a reliable basis for further interpretation of the nucleation, growth, and development of C-S-H from *in situ* IR spectra of cement hydration, which will be the focus of a separate manuscript in our investigation.

For this purpose, IR spectra of synthetically produced C-S-H phases are compared with bulk spectra of some dimeric and single-chain crystalline phases. Polarized single-crystal IR spectra of synthetic jaffeite, 14 Å tobermorite and jennite are used to provide straightforward assignment of the vibrational modes.

2. Samples and methods

2.1. Samples

2.1.1. Synthetic C-S-H samples

Synthetic C-S-H samples were synthesized from freshly prepared CaO (from $CaCO_3$ p.a., Merck at 1000 °C), highly disperse SiO_2 (Aerosil, Evonik) and distilled H_2O following the procedure described elsewhere [16]. Samples with target C/S ratios of 2/3, 3/4, 5/6, 1/1, 6/5, 4/3 and 3/2 were prepared mechanochemically.

2.1.2. Synthetic crystalline C-S-H samples

14 Å tobermorite, $Ca_5Si_6O_{16}(OH)_2.7H_2O$, was synthesized hydrothermally in Teflon-lined stainless-steel autoclaves at 65 °C for 8 months using C-S-H phase with C/S = 1 as a starting material. Jennite, $Ca_9Si_6O_{18}(OH)_6{\cdot}8H_2O$, was prepared following a similar procedure, but with a C-S-H phase with C/S = 3/2. Jaffeite, $Ca_6[Si_2O_7](OH)_6$, was synthesized from triclinic C_3S treated hydrothermally for 1 week at 250 °C. Killalaite, $Ca_3[Si_2O_6(OH)](OH)$, was synthesized from CaO and Aerosil in stoichiometric ratio of 1.5 at 240 °C for 4 weeks. Cuspidine, $Ca_4Si_2O_7(F,OH)_2$, was prepared hydrothermally at 200 °C for 24 h with starting materials fine-ground industrial quartz, $Ca(OH)_2$ and CaF_2 (16 wt%) mixed at a C/S ratio of 2.

2.2. Methods

2.2.1. IR bulk spectra

IR bulk spectra of the crystalline phases were measured in transmission on KBr pellets using a TENSOR 27 spectrometer (Bruker Optics, Ettlingen, Germany) equipped with a deuterated triglycine sulfate (DTGS) detector. The spectral range was 400–3800 cm $^{-1}$ and the spectral resolution 2 cm $^{-1}$. The IR measurements of the synthetic C-S-H phases and the *in situ* measurements of CEM I hydration were performed on a TENSOR II spectrometer (Bruker Optics, Ettlingen, Germany) with a DTGS detector and a golden gate ATR cell with diamond crystal (Specac LTD, Orpington, UK). A specially developed sample holder for *in situ* hydration measurements was used (Fig. SI1A). Spectra with 64 scans were acquired every 2 min in the range 400–4000 cm $^{-1}$ with a spectral resolution of 2 cm $^{-1}$.

2.2.2. IR polarized spectra

Synchrotron-based infrared spectroscopic experiments were conducted on the IR2 beamline of the KIT Light Source using synchrotron IR light from the 2.5 GeV storage ring KARA (Karlsruhe, Germany). Spectra were acquired under ambient conditions with an IFS 66v/S (for jaffeite) and Vertex 80v (for 14 Å tobermorite and jennite) FTIR spectrometer, coupled to an IRscopeII microscope (Bruker Optics GmbH, Ettlingen, Germany).

The measurements were performed in transmitted-light mode using Schwarzschild objectives (36×, 0.5 N.A.), with an 8 μm aperture for jaffeite and jennite, and a 12.5 μm aperture for 14 Å tobermorite. A liquid nitrogen-cooled MCT (HgCdTe) detector and a KBr beamsplitter were used. The microscope enclosure box was purged with dry nitrogen gas to reduce humidity to approximately 2 %.

Single crystals of jaffeite (32 μm long and 1.5 μm thick, see Fig. 4A), 14 Å tobermorite (20 μm long and 8 μm thick, see Fig. 5, left), and jennite (30 μm long and 3 μm thick, see Fig. 9) were placed on a type IIa diamond window inside a rotation stage (SmarAct GmbH, Oldenburg, Germany). Mid-infrared spectra were recorded with 512 accumulations at an 80 kHz scanner velocity and a spectral resolution of 4 cm $^{-1}$.

To eliminate the influence of the decay of the synchrotron electron beam current, background spectra were recorded through the bare diamond sample holder prior to each sample measurement and were subsequently used for the calculation of absorbance data. The high brilliance of the synchrotron infrared beam allowed us to set the diameter sensed by the detector to 8 μm, which is smaller than the

diffraction limit in the long wavelength range (14.3 μm at 700 cm ^{1}), while still attaining a good signal-to-noise ratio. The beam direction was perpendicular to the *ac*-plane of the jaffeite and to the *ab*-planes of the 14 Å tobermorite and jennite crystals.

To examine the dependence of the vibrational bands on the polarization of the incident light, a KRS5 polarizer (Specac Ltd., Orpington, UK) was placed in front of the sample, with the direction of the electrical vector **E** kept parallel to the X-axis of the microscope stage for all measurements. The polarization angle dependence was achieved by rotating the sample stage. To improve the signal-to-noise ratio, eight spectra were recorded at each angle step and subsequently averaged. The positions of the IR bands were determined by processing the experimental data using OPUS v8.5 software.

2.2.3. Raman spectroscopy

Raman spectroscopy on single crystals of 14 Åtobermorite and jennite was applied on a LabRam ARAMIS (Horiba Jobin Yvon GmbH, Oberursel, Germany) combined with BX41 optical microscope equipped with polarizers. An excitation wavelength of 473 nm at a laser power of 10 mW (measured on the sample) was used. For maximal lateral and axial resolution a 100× objective (NA = 0.9) was utilized. The spectral resolution with the 1800 groves/mm grating was better than 1 cm ^{1}. A self-made device was used for sample tilting (Fig. SI1B).

2.2.4. NMR

The NMR spectra were recorded on a Bruker ASX 400 NMR spectrometer equipped with a 9.397 T widebore superconducting magnet. ^{29}Si MAS NMR measurements were carried out at 79.49 MHz using a standard Bruker 7 mm MAS probe with sample spinning at 4.0 kHz, a single pulse duration of 3 μs (90° pulse length 5.8 μs) and proton decoupling. 200–400 scans were accumulated with a 120 s recycle delay. To ensure that the 120 s delay is sufficient with regard to the spin-lattice relaxation time (T1), some experiments were repeated with a delay of 240 s, but no change in intensity could be observed. Tetramethylsilane was used as the reference standard for ^{1}H and ^{29}Si. Spectra were processed with zero filling and 30 Hz exponential line broadening. Spectra were fitted using Dmfit2003 [13] (Table SI1).

2.2.5. Trimethylsilylation (TMS)

Silicate speciation was determined by TMS followed by gas chromatography with flame-ionization detection (GC-FID), as described by Hoebbel et al. [14]. 10 mg of solid material were dissolved and silylated for 15 min in a continuously stirred mixture of 10 mL dimethylformamide, 8 mL hexane, and 2 mL trimethylchlorsilane (TMS) at 20 °C. Under continuous stirring 420 mL of water was added. The solution was then injected into the GC-FID system, which consisted of an Agilent 5890 gas chromatograph equipped with a 30 m capillary column DB1HT. The GC analysis was carried out in constant pressure mode (25 psi) using an oven temperature program with a heating rate of 12 °C/min in the range from 80 °C to 340 °C. Retention times (minutes) were as follows: $(TMS)_4SiO_4$: 4.23, $(TMS)_6Si_2O_7$: 9.45, $(TMS)_8Si_3O_{10}$: 14.08, $(TMS)_{10}Si_4O_{13}$: 18.02, $(TMS)_{12}Si_5O_{16}$: 21.38. The expected yield is 80 % with a relative error of ±10 %. Samples with low SiO_2 yield were measured in duplicate, while those with high SiO_2 yield were measured 2–4 times (Table SI2).

All structure images were generated using CrystalMaker® (CrystalMaker Software Ltd., Oxford, England, www.crystalmaker.com).

3. Results and discussion

3.1. Silicate speciation of the synthetic C-S-H phases

The synthesized C-S-H samples were also investigated by ^{29}Si NMR (Fig. 1A) and TMS (Fig. 1B), providing comprehensive understanding of the silicate speciation. Tabulated data are given in the SI file. The NMR results are identical to the data from [15] where C-S-H phases were synthesized using a similar procedure. It is evident that samples 4/3 and 3/2 are dominated by Q^1 in NMR, resulting in 19 wt% of the total SiO_2 found by TMS (25–26 % from the expected 35-32 wt%, respectively) in dimeric species. Pentamers sum up to 3 wt% and 4 wt% in C/S = 3/2 and 4/3 sample, respectively. It should be considered that pentamers are built from 2 Q^1 and 3 Q^2 tetrahedra, thus further contributing strongly to Si-O_{nbr}, having O_{nbr}/O_{br} = 12/4. The higher number of O_{nbr} in Ca-rich samples is well reflected by XPS performed on similar samples [16]. The sample with C/S = 1/1 shows an increased Q^2 contribution, mostly assigned to longer chain species along with pentamers. Q^1(NMR) and the corresponding quantity of dimers (TMS) decreases. Samples 2/3 and 3/4 are mostly composed of chain-like species (Q^2) not measurable by TMS. The results are consistent with the generally accepted idea that the silicate polymeric species present in C-S-H obey the rule $Si_{(3n\ 1)}\ O_{(3(3n-1)+1)}$, thus excluding presence of trimers and tetramers [17–19]. The small differences in the chemical shifts of the Q^1 species from 78 ppm to 80 ppm with decreasing C/S are due to the decrease in the quantity of dimers and the corresponding increase in chain ends, which possess different environments having Q^2 tetrahedra as neighbors. A similar case is observed for the Q^2 species shifting from 84 ppm to 86 ppm

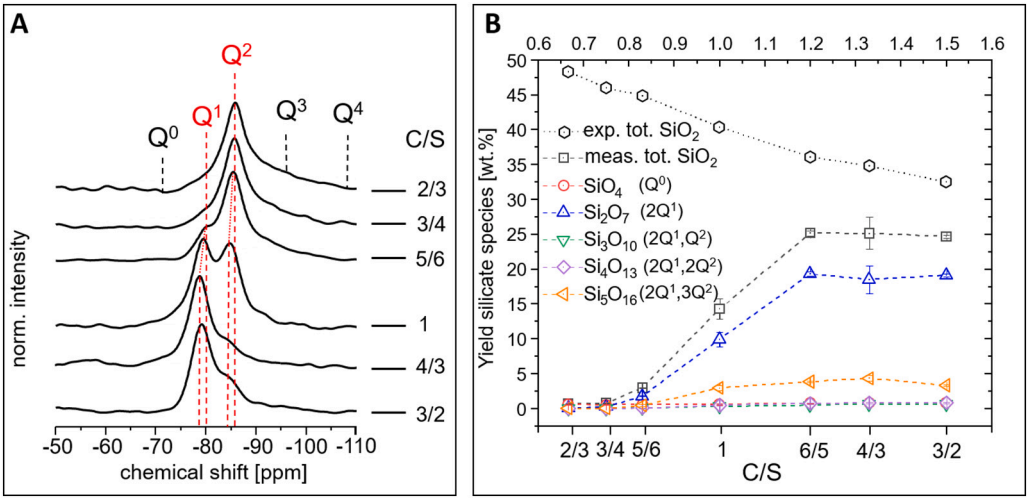

Fig. 1. A: ^{29}Si NMR spectra and B: results of the speciation with TMS of the nanocrystalline C-S-H phases. Samples 3/2 and 4/3 are dominated by Q^1 species with small contributions of pentamers $2Q^1/3Q^2$. Sample 1 shows increased Q^2 contribution mostly assigned to longer chain species along with pentamers. Q^1 (NMR) and the corresponding quantity of dimers (TMS) decreases. Samples 2/3 and 3/4 are mostly composed of chain-like species (Q^2) not measurable by TMS.

upon changing from dominating pentamers to longer chains between C/S = 1 and C/S = 5/6. Similar considerations made in [15] are confirmed by combination with the TMS results.

3.2. Band assignment of the C-S-H phases: general remarks with reference to literature data

As already mentioned in the introduction, the assignment of IR bands in the literature is based on the study by Yu et al. [11], which provides valuable information about the IR spectra of C-S-H phases and bulk spectra of 14 Å tobermorite and jennite, not only in the MIR, but also in FIR and NIR ranges. However, there is still an inconsistency about the attribution and interpretation of individual Si—O bands. In addition, the polymerization degree of the silicate units in C-S-H phases in terms of Q^{1-2} is a subject of discrepancies. For example, Yu et al. [11] and Higl et al. [9] agree in attributing the band at 979/940 cm ^{1} to Q^2, the band at 811/815 cm ^{1} to Q^1, and a shoulder at 1010 cm ^{1} also to Q^1 silicate units. In contrast, John and Stephan, [10] assign these bands to modes of Q^1 silicate units. They demonstrated a strong dependency of the development of one or more silicate species on the C/S-ratio of the sample.

One of the most troubling problems is the preprocessing of the *in situ* IR spectra and its possible influence on band intensities. For example, in the work of Higl et al. [9], the main band of C-S-H is positioned at 1005 cm ^{1} after the preprocessing procedure. Further, the authors state: "… the difference in time of their growth also leads us to assign the band at 945 cm ^{1} to Q^2-silicate species and the band at 1005 cm ^{1} to Q^1-silicate species, as expected for the formation of longer silicate chains starting from dimeric silicate units. This is supported by the spectra measured for synthetic C-S-H by Yu et al. [11], where a shoulder slightly above 1000 cm ^{1} becomes more pronounced with higher C/S ratios as does the established band of Q^1 silicate species at 811 cm ^{1}." Therefore, the authors claim that initially, the band at 1005 cm ^{1} grows, assigned to Q^1 (dimeric species), followed by the band at 950 cm ^{1} belonging to more polymerized (Q^2) silicates. A quick check with the data of Yu et al. [11] and Fig. 2 shows an obvious inconsistency. In Fig. 2, IR spectra of synthetic C-S-H phases with C/S varying between 3/2 and 2/3 are compared with *in situ* IR spectra of hydrated OPC after 8 h, 24 h, 48 h and 96 h. Clear resemblance between both is seen not only at the beginning of C-S-H formation, but also at later stages. In the presented range, the band at 1111 cm ^{1} is due to ν_3-SO_4 stretching of ettringite. A small shift of the main band from 940 cm ^{1} (8 h) to 944 cm ^{1} (96 h) is observable. It should be considered that Al incorporation in C-S-H during cement hydration would shift the main Si—O stretching band to higher frequencies (due to higher polymerization *via* entering of Al in bridging sites) as observed in IR spectra of C-A-S-H [20–22]. Nevertheless, it seems unlikely to occur in early stages, when Al is primarily involved in the formation of Aft and AFm phases. Not only in the cited work of Higl et al. [9], but also elsewhere, a shift to higher frequencies of the main Si—O stretching band is interpreted as an increase in the polymerization of the silicate species [23]. However, this is unlikely to happen during the early hydration period. Even the opposite trend is expected. It is generally accepted that the C-S-H nuclei are rather low in Ca content with increasing C/S from core to rim upon growth [24–26]. Furthermore, the formation of a protective Si-rich layer, explaining the presence of the induction period, is proposed. Therefore, it is not justified to interpret possible frequency shifts as polymerization of the silicate species.

During initial cement hydration, heterogeneous nucleation and

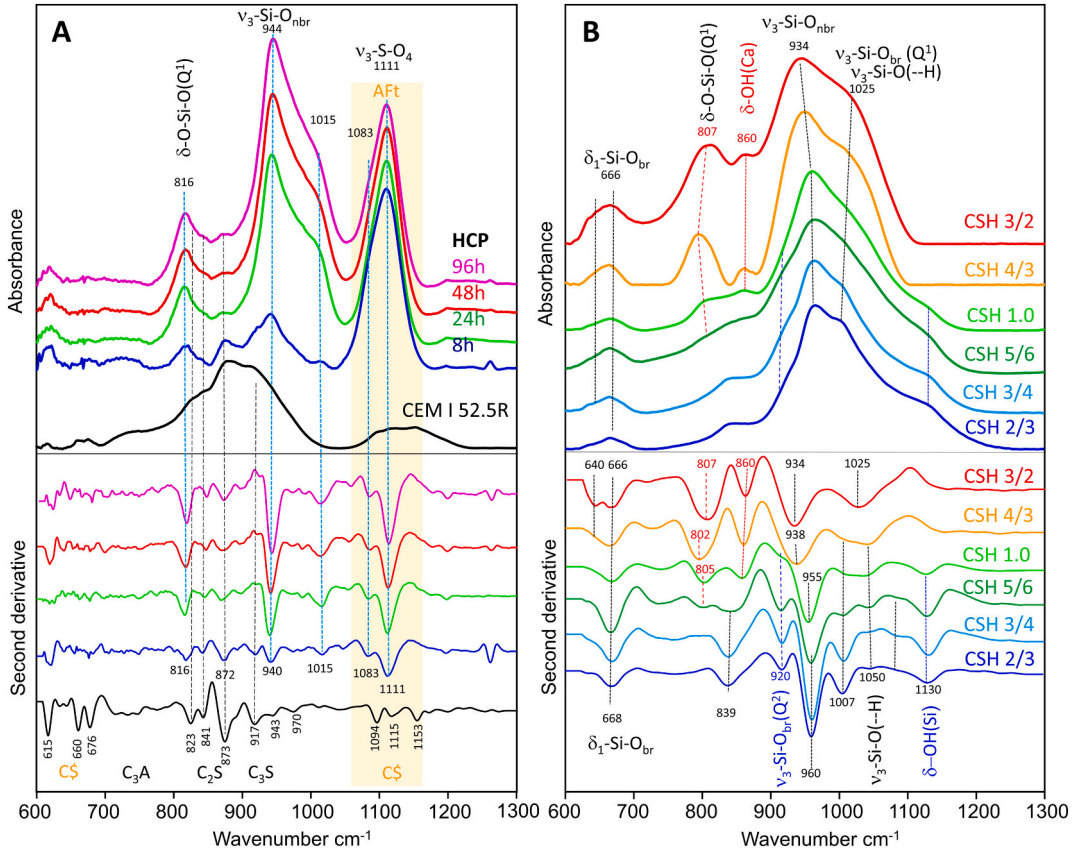

Fig. 2. A: *In situ* IR spectra of hydrated OPC after 8 h, 24 h, 48 h and 96 h along with unhydrated CEM I (C$-anhydrite). Second derivative of the absorbance was used for evaluation of the band positions (bottom). B: IR spectra of synthetic C-S-H phases with C/S ratios ranging from 3/2 to 2/3 (top). Red dashed lines show presence of bands typical for dimeric species. Blue dashed lines show presence of bands typical for chain-like silicate species. Second derivative of the absorbance spectra (bottom). (For interpretation of the references to color in this figure legend, the reader is referred to the web version of this article.)

growth of the C-S-H phases are controlled by lime concentration. It is expected to take place primarily at the surface of clinker particles where the latter is lower [25 and references therein]. In the early stages, there is plenty of free space, but as hydration progresses, the autocatalytic exponential growth of C-S-H intercalated with portlandite leads to steric hindrance in later stages [26]. Regarding the free space, it is evident that there must be a significant difference between hydration of C_3S and OPC due to the rapid nucleation and growth of ettringite in the latter. As hydration proceeds, the concept of growth of LD C-S-H and HD C-S-H further complicates the picture, differentiating in spatial distribution, porosity, and H_2O content [27,28].

In another *in situ* IR study, Ylmen et al. [8] provide very limited information about the assignment of the C-S-H bands. Their approach of using intensity of the bands, instead of peak area, which would better reflect the real situation, leads to several inconsistent conclusions when directly compared with calorimetric data. In particular, their claim that a band at 1350 cm ^{1} should be assigned to a combination of Si—O stretching and Si-OH bending seems inexplicable.

In addition, there are also some aspects that have not been considered so far. These include the possible influence of particle size on the positions of absorption bands and the consideration of Si—O bridging and non-bridging modes. Regarding particle size, it is helpful to refer to numerous works on X-ray amorphous materials, such as SiO_2 glasses. The spectra of such materials show surface phonon modes, whose positions seem to increase in frequency with increasing particle size [29]. Therefore, the interpretation of the increasing band frequency with hydration time must be carefully considered. The small shift toward higher frequency in the first 24-96 h is possibly due to the increase of the particle size until growth is hampered by the confined space. Furthermore, the densification of the microstructure would lead to a further high-frequency shift as observed in the annealing of SiO_2 gels. Therefore, the growth rate and quantity of the C-S-H phase cannot be estimated solely by the intensity and position of the main Si—O stretching band.

3.3. Bulk IR spectra of C-S-H phases

Fig. 2B shows the IR spectra of synthetic C-S-H phases with C/S varying between 3/2 and 2/3. In Fig. 3, IR spectra of Ca-rich C-S-H phases alongside those of various crystalline phases consisting of Si_2O_7 units: jaffeite, cuspidine, killalaite and rankinite listed in order of decreasing C/S ratio are presented. Additionally, the spectra of chain silicates jennite and 14 Å tobermorite are shown. The frequencies of the individual bands alone are insufficient to differentiate between Q^1 and Q^2 without considering the entire spectrum.

The band at 666 cm ^{1} unambiguously corresponds to the δ-Si-O-Si mode, which is also observed in the Raman spectra [11,30,31], although some stretching is inevitably involved. A broad band at 807 cm ^{1} with maximal intensity is present in the spectra of Ca-rich samples as previously reported [11], and it was attributed to Si—O stretching of Q^1, without any explanation of the mode behind it. In several studies, changes in the intensity of this band have been successfully interpreted as reflecting an increase or decrease in the number of dimeric species, influenced by alkali or the incorporation of Al, respectively [22,32]. The band can be traced to the spectrum of the C/S = 5/6 phase, but the maximal intensity shifts to 839 cm ^{1}. The band at 839 cm ^{1} is clearly visible in the spectra of C/S = 3/4 and 2/3 samples albeit with considerably lower intensity compared to the 807 cm ^{1} band discussed previously. An examination of the spectra of the crystalline compounds with dimeric structures reveals presence of similar band(s) in all of them, confirming the involvement of Q^1 dimers. This observation aligns well with the decrease in the number of the dimeric species in sample C/S = 1 as seen in TMS and the increased proportion of Q^2 species in NMR. The fact that a small shoulder at about 810 cm ^{1} is still visible in the IR spectrum of the C/S = 5/6 sample, indicates a small but still measurable quantity of dimers in this sample (Fig. 2B). The band with very low

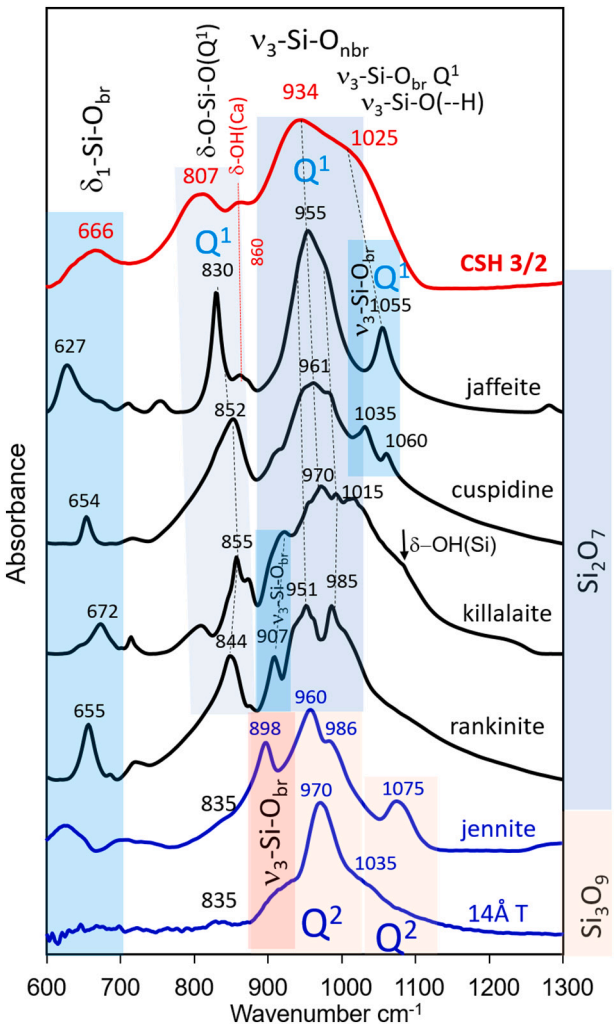

Fig. 3. IR spectra of various Ca-diorthosilicates (black) and chain silicates (blue). It is noted that the ν_3 Si—O modes of Q^1 and Q^2 are indistinguishable. For comparison, the spectrum of C-S-H with C/S 3/2 is shown in red. (For interpretation of the references to color in this figure legend, the reader is referred to the web version of this article.)

intensity at around 860 cm ^{1} seen in the spectra of the Ca rich synthetic C-S-H phases (C/S = 1/1–3/2) and at slightly lower frequency in the hydrated OPC (Fig. 2A) corresponds well to the liberation of OH groups bonded explicitly to Ca. All existing models predict their presence in C-S-H phases [19,33].

To introduce more clarity regarding the band assignments, it is helpful to reference the works of Lazarev and Dowty for assignment of Si—O bands in diorthosilicates and chain silicates [34–37]. These assignments are based on the knowledge of Si-O-Si bond angles and distances, which determine the force constants. Additional background information is provided in the SI. Firstly, it is important to consider that due to the lack of long-range order there is a violation of the selection rules similarly to glass materials [38,39]. Therefore, it is possible to obtain bands for all symmetric and antisymmetric modes of Si—O vibrations. The next step is to properly assign these bands, considering not only the degree of silicate polymerization in terms of Q^1 and Q^2, but also the contributions of Si-O_{nbr} bonds. The main silicate species formed during early cement hydration is clearly a dimer of the type Si_2O_7 and $Si_2O_{7-x}(OH)_x$ where x can vary between 0 and 2 [33,40].

Numerous studies [34,36,37] have shown that when the Si-O-Si angle is 180°, the Si-O_{br} stretching frequency is expected to be higher than that of the Si-O_{nbr} stretching due to the exact saturation of the

bridging oxygens, which have only two Si neighbors. On the other hand, the Si-O-Si angle in C-S-H is known to be very close to that in 14 Å tobermorite [31,41] being approximately 138°. This angle is likely maintained from the beginning of C-S-H nucleation, corresponding to minimal binding energy, as seen in studies of H_3Si-O-SiH_3 complexes [42]. As a result, the O_{br} is oversaturated in terms of Pauling electronic valence rule [37] and the O_{nbr} are possibly underbonded. Therefore, it is to expect that bands in the higher frequency part of the Si—O envelope are due to Si-O_{nbr} antisymmetric stretching, while those in the lower frequency part are due to Si-O_{br} antisymmetric stretching (see SI for details).

The order of spectra of the dimeric crystalline compounds in Fig. 3 varies from top to bottom, not only by decreasing C/S ratio, but also by the Si-O-Si angle: 180° (jaffeite, $Ca_6[Si_2O_7](OH)_6$ [50]), 155.4° (cuspidine, [43]), 137.2° (killalaite, [44]) and 136.2° (rankinite [45]). The 180° Si-O_{br}-Si angle in jaffeite allows for a clear assignment of the band at 1055 cm^{-1} to ν_3-Si-O_{br} according to Dowty's theory. Direct proof will be presented later in this paper. Cuspidine has overbonded O_{br} which is additionally shared with two Ca atoms. Therefore, it is to expect that the Si-O_{nbr} bond vibrates at higher frequency due to being underbonded. Indeed, two of the O_{nbr} are shared with three Ca, and four are shared with only two Ca atoms. The shorter Si-O_{nbr} bond length (1.60 Å) compared to Si-O_{br} (1.66 Å) justifies the assignment of ν_3-Si-O_{nbr} at higher frequency. Killalaite exhibits additional Si-OH environments, which complicate the band assignment and generally result in higher Si—O vibrational frequencies. This deviation from the established correlation between silicate polymerization degree and vibrational frequency [46] is anticipated and discussed in [47].

Rankinite similar to cuspidine, has overbonded O_{br} with long Si-O_{br} (1.66–1.68 Å) and short Si-O_{nbr} (1.59–1.60 Å), allowing the high-frequency part of the envelope to be assigned to ν_3-Si-O_{nbr}. Dowty's computational work [37] supports this assignment attributing bands around 950 cm^{-1} mostly to Si-O_{br} and those around 985 cm^{-1} to Si-O_{nbr} stretching (Fig. 3).

In chain silicates, bridging oxygens are more constrained leading to Si-O_{nbr} stretching occurring at higher frequency than Si-O_{br}. This is evidenced by polarized spectra of 14 Å tobermorite and jennite, which enable direct assignment of observed bands to specific vibrational modes. These assignments will be discussed in detail later.

The intrinsic disorder of the C-S-H suggests presence of multiple environments of Si_2O_7 species particularly those with silanol groups. The higher number of the Si-O_{nbr} bonds and the higher intensity of the band at approx. 934–960 cm^{-1} in their IR spectra (Fig. 2A, B), conclusively indicate that this band arises from ν_3-SiO_{nbr} modes.

Furthermore, as polymerization increases with decreasing C/S, which is coupled to the presence of Ca vacancies in the interlayer, it is expected that more silanol environments are required to maintain the charge balance. This could explain the higher absorption observed around 1130 cm^{-1} (Fig. 2B).

3.4. Polarized spectra

3.4.1. Jaffeite: $Ca_6[Si_2O_7](OH)_6$

To obtain a more reliable assignment of the IR bands to specific modes, we use polarized single-crystal IR spectra of jaffeite, 14 Å tobermorite, and jennite, taken with synchrotron radiation. For the exact assignment of the vibration mode of the C-S-H band at approx. 807 cm^{-1}, which belongs to Q^1 (Figs. 1 and 2), we choose jaffeite as a model due to its higher symmetry and resulting simple IR spectrum.

Previous studies of the bulk spectra of jaffeite report three main bands in the Si—O stretching region at 831 cm^{-1}, 951 cm^{-1}, and 1050 cm^{-1}, all assigned to ν_3 Si—O modes [48].

Fig. 4A shows the polarized spectra of a jaffeite single crystal. Jaffeite, $Ca_6[Si_2O_7](OH)_6$ crystalizes in the P3 space group according to [49] and forms prismatic crystals along the *c*-axis (SI file, Fig. SI2). Along the *c*-axis linear Si_2O_7 groups are oriented with Si-O-Si angle = 180° (Fig. 4B).

In the spectrum polarized along the *c*-axis ($\vec{E} \| c$), two bands are observed in the range 700–1200 cm^{-1}. We assign the band at 1049 cm^{-1} to ν_3-Si-O_{br} antisymmetric stretching along the Si-O_{br}-Si line (blue arrows). In the spectrum polarized perpendicularly to the *c*-axis ($\vec{E} \perp c$), a single asymmetric band is centered at 968 cm^{-1} with a shoulder at about 980 cm^{-1}. This band can be unambiguously assigned to ν_3-Si-O_{nbr} stretching due to the orientation of the Si_2O_7 group, which results in a significant component of the Si-O_{nbr} vibration along this direction (green arrows). As expected, the spectrum taken at 45° to the *c*-axis is a combination of all bands and exhibits the characteristics of the bulk

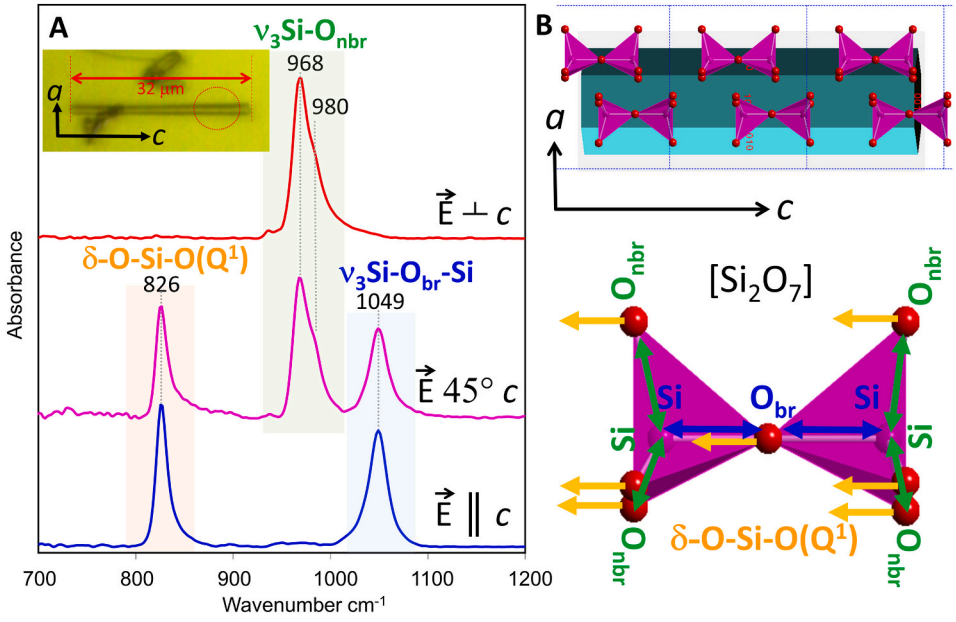

Fig. 4. A: Polarized IR spectra of jaffeite. Spectrum taken with **E**$^{\perp}$*c*-axis (red), **E** at 45° to the *c*-axis (magenta), and **E**$\|$*c*-axis (blue). B: Orientation of the dimeric species along the *c*-axis of jaffeite with corresponding vibrational mode: ν_3-Si-O_{nbr} (green arrows), ν_3-Si-O_{br} (blue arrows), Si—O "rattling" (orange arrows). (For interpretation of the references to color in this figure legend, the reader is referred to the web version of this article.)

spectrum shown in Fig. 3. Considering the band at 826 cm ^{1} in the $\vec{E} \| c$ spectrum, it is evidently strongly polarized and conjugated with the Si-O_{br}-Si stretching. Some authors attribute bands in this region to coupled ν_3-SiO_{3nbr} + γ-Si-O-Si (out-of-plane) bending [50] in Ca_2Zn-Si_2O_7. However, this is not applicable here due to complete polarization, resulting in the absence of absorption in the polarization plane perpendicular to the Si-O-Si plane. In their study of different polymorphs of $Y_2Si_2O_7$, Diaz et al. assigned a similar band to the multiple stretching of all Si—O bonds in the diortho unit [51]. Reflecting on this assignment and considering the observations in Fig. 4, we propose that the band at 826 cm ^{1} arises from the simultaneous movement of all seven oxygens against the two Si atoms along the *c* direction of jaffeite (orange arrows), which comprises the channels embedding the Si_2O_7 groups. O_{br} movement in this direction corresponds to the antisymmetric stretching ν_3-Si-O_{br}, explaining the conjugate nature between the bands at 826 and 1049 cm ^{1}. Similar mode is sometimes described as "rattling" of Si within the "oxygen cage". Applying this assignment to the spectra of hardystonite in [50] perfectly matches the observed polarization spectra. As expected, this mode is absent in the direction perpendicular to *c*. Fig. 3 confirms that in the IR spectra of dimeric silicates, a band in the range of 800–860 cm ^{1} is always present. These bands are generally broader than that of jaffeite due to the lower symmetry (mostly monoclinic) of the silicates presented. Therefore, we assign the band at 807 cm ^{1} in the spectra of the Ca-rich C-S-H phases to a group vibration τ-O_7-Si_2 or "rattling" of the oxygen atoms in Si_2O_7 species along the Si—Si direction. Strictly speaking, this band is a combination of ν_4-Si-O_{nbr}/ν_3-Si-O_{br}. However, since it includes changes of all O-Si-O angles in antiphase, we will refer to it as δ-O-Si-O for brevity (Figs. 4 and SI3). Due to its asymmetric nature, this mode is not expected to appear in the Raman spectrum of jaffeite, which is indeed the case. This band is observed, as expected, only in Ca-rich C-S-H phases, as stated by [11] and seen in our own IR spectra (Fig. 2). As the ratio of O_{nbr}/O_{br} in Si_2O_7 dimers is quite high (=6), the O_{nbr} dominate the δ-O-Si-O (ν_4-Si-O_{nbr}/ν_3-Si-O_{br}) vibration.

Comparing the IR spectrum of synthetic C-S-H with a C/S ratio of 3/2 to those of jaffeite, cuspidine, killalaite, and rankinite (all possessing Si_2O_7 units) reveals close similarities in band positions and assignments (Fig. 3) including the δ-O-Si-O vibration. As polymerization increases, the number of Si-O_{nbr} bonds decreases, resulting in reduced intensity of this band. Additionally, the frequency shifts, reaching 835 cm ^{1} in the spectra of 14 Å tobermorite and jennite (shoulder). The movement of O_{nbr} in chain silicates not only results in lower intensity but also occurs in a different direction compared to dimeric structures. As demonstrated later for 14 Å tobermorite, the band at 834 cm ^{1} is associated with a different nature, specifically related to Si(OH) interactions.

3.4.2. 14 Å tobermorite: $Ca_5[HSi_3O_9]_2 7H_2O$

3.4.2.1. IR polarization spectroscopy. A key to determining the vibrational modes based on crystal direction is provided once again by polarized spectra. The IR spectra of a single 14 Å tobermorite crystal (20 μm along the *b*-axis), oriented along [001], are presented in Fig. 5. Proof of the orientation of the crystallographic axes of 14 Å tobermorite and its morphology, as provided by SAED (TEM), is included in the Supplemental Information file (Fig. SI4). The triple single chain ("dreier-einfachkette") in 14 Å tobermorite is characterized by the regular sequence of two paired tetrahedra and one bridging tetrahedron sharing oxygens (O_{br}). Accordingly, Si atoms are differentiated here into Si_p (Si in paired tetrahedra) and Si_{br} (Si in the bridging tetrahedron). The two remaining non-bridging oxygens (O_{nbr}) involved in tetrahedral coordination have different environments depending on whether they belong to Si_p or Si_{br} tetrahedra.

In polarization perpendicular to the elongation (E ⊥ b), the main contribution to the IR spectrum arises from the ν_3-Si-O_{nbr} vibrations (orange/blue arrows). We can distinguish between the Si_p-O_{nbr} vibrations of the paired tetrahedra (light blue) and those belonging to Si_{br}-O_{nbr}. The former are more numerous and are characterized by a uniform environment of the O_{nbr}, with each O_{nbr} being shared by three Ca atoms, each belonging to the complex layer. The dipole moment of only one of the two Si_{br}-O_{nbr} bonds is aligned with the oscillation direction of the electric vector of the polarized IR light. The second Si_{br}-O_{nbr} bond is not probed in this experimental geometry, as it is parallel to the direction of IR light propagation (along *c* and perpendicular to the *ab* plane). Both O_{nbr} atoms in the bridging tetrahedron have completely different environments: one (O6) is coordinated by a Ca atom from the intralayer (Ca-O_{nbr} = 2.75 Å), while the second is coordinated by two Ca atoms from the interlayer (O5). The shared oxygen with the Ca from the complex layer is also hydroxylated. Compared to the O_{nbr} atoms in the paired

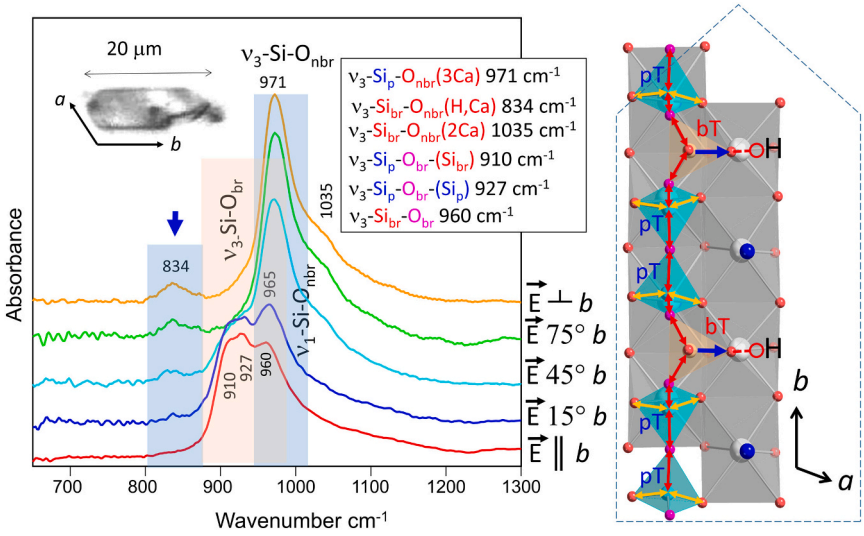

Fig. 5. Polarized IR spectra of 14 Å tobermorite with the propagation direction of the IR synchrotron light along [001]. Left: Spectra taken with **E**IIb (red), **E**15°b (blue), **E**45°b (light blue), **E**75°b (green), and **E**⊥ b-axis (orange). The mode assignment is listed in the square. The crystal was lying in the ab-plane. Right: Schematic view of the crystal structure in the same orientation as in the experiment. Si-O_{nbr} (orange arrows), Si-O_{br} (red arrows), orientation of the Si-O(H) stretching vibrations (blue arrows). Paired tetrahedra (pT, light blue), bridging tetrahedra (bT, light orange), Ca-polyhedra (grey), O_{nbr} (red circles), O_{br} (magenta circles), H_2O (blue). Schematic outline of the contours of the crystal (dashed line). (For interpretation of the references to color in this figure legend, the reader is referred to the web version of this article.)

tetrahedra, these atoms are clearly underbonded, (showing bond valence anionic sum charges of 1.57 (O5) and 1.03 (O6) compared to 1.83–1.91) [41]. As a result, they are expected to vibrate at higher frequencies. Notably, the Si2-O5 bond is the shortest among all Si—O bonds, measuring 1.57 Å, which further supports the expectation of a higher vibrational frequency. Therefore, we assign the band at 971 cm ^{1} to ν_3-Si$_p$-O$_{nbr}$ and the shoulder at 1035 cm ^{1} to ν_3-Si$_{br}$-O$_{nbr}$. In the same orientation, we observe a low-intensity band at 834 cm ^{1}, which corresponds to the group movement of oxygen against silicon. Due to the chain structure, the oxygen movement seems to be constrained in the *b*-direction, occurring mostly perpendicular to it. In polarized spectra along the *b*-axis the dominating contributions arise from the ν_3-Si-O$_{br}$ stretching vibrations. The bands at 834 cm ^{1} and 1035 cm ^{1} appear to be conjugated, suggesting another possible explanation: both bands may be associated with the presence of an oriented OH group.

Vidmer et al. [12] calculate an IR absorption band at 815 cm ^{1}, assigning it to Si—O stretching (OH–SiCa in bridging tetrahedra). This assignment appears reasonable, as in our IR polarized spectra this mode (observed at 834 cm ^{1}) shows a significant component only in the spectrum recorded with the polarization vector perpendicular to the *b*-axis. In the high frequency part of the envelope the authors calculate a band at 1060 cm ^{1} which they assign to the Si$_p$-O$_{br}$-(Si$_{br}$), which corresponds to O—Si$_2$ according to their nomenclature, but relate it with an experimental band at 1120 cm ^{1}. This seems doubtful considering the following discussion.

We can distinguish three types of Si-O$_{br}$ bonds in the structure, Si$_p$-O$_{br}$ shared between paired tetrahedra, Si$_p$-O$_{br}$ shared between Si$_p$ and Si$_{br}$ and Si$_{br}$-O$_{br}$ shared between Si$_{br}$-Si$_p$ tetrahedra [41]. Accordingly, three bands are observed. From the structural scheme in Fig. 5 (right), it can be seen that the former two are oriented almost parallel to the *b*-axis (vertical red arrows), while the latter are inclined at approximately 30° to the *b*-axis. As the polarization angle increases from 0° (**E**||*b*) to 15° (**E**15°*b*), we observe an increase of the intensity of the band at approx. 960 cm ^{1}. Therefore, we assign this band to ν_3-Si$_{br}$-O$_{br}$ mode. The higher frequency of this mode is expected, given that these bonds are the shortest (mean = 1.615 Å) compared to the other Si-O bonds (1.65 Å and 1.67 Å). The band at 927 cm ^{1} could be predominantly assigned to ν_3-Si$_p$-O$_{br}$ shared between paired tetrahedra (ν_3-Si$_p$-O$_{br}$-(Si$_p$) in the figure), having the highest component in the orientation (**E**||*b*). The band at 910 cm ^{1} could correspondingly be assigned to ν_3-Si$_p$-O$_{br}$ shared between paired and bridging tetrahedra, ν_3-Si$_p$-O$_{br}$-(Si$_{br}$), in contrast with the assignment by Vidmer et al. [12], who use this assignment for the 1060 cm ^{1} band as mentioned above. Interestingly, the authors calculate a band at 930 cm ^{1} but assign it to (O\SiCa$_x$, O\Si$_2$) (using their nomenclature) and connect it to the observed band at 965 cm ^{1}. The assignment is correct as they mean the ν_3-Si$_p$-O$_{nbr}$ (971 cm ^{1}), stating that it is the main band in the IR spectra. At the same frequency, they assign Si$_{br}$-O (not differentiating between O$_{br}$ and O$_{nbr}$, but it is to assume that they mean O$_{br}$). While this assignment seems generally correct, applying polarized IR spectroscopy helps to differentiate between the Si$_p$-O$_{nbr}$ (971 cm ^{1}) and Si$_{br}$-O$_{br}$ (960 cm ^{1}) modes. Additionally, both bands due to Si$_p$-O$_{br}$-(Si$_p$) at 927 cm ^{1} and Si$_p$-O$_{br}$-(Si$_{br}$) at 910 cm ^{1} are not resolved in the calculations. The general observation that the Si$_p$-O$_{nbr}$ vibrations occur at higher frequencies than those of Si-O$_{br}$ is confirmed (and expected) based on the shorter bond lengths calculated from the structure of the 14 Å tobermorite [41]. The shoulder at 1035 cm ^{1} is likely connected to Si$_{br}$-O$_{nbr}$-(2Ca) vibration of the second O$_{nbr}$ (O5 according to[41]).

The position of the hydrogen in the silanol group of 14 Å tobermorite was not determined by Bonaccorsi et al. However, based on the IR polarized spectra, we assume that the O—H bond is oriented perpendicular to the *b*-axis. To determine more precisely the orientation of the OH group, we will also discuss the polarized Raman spectra in the following.

3.4.2.2. Raman polarization spectroscopy. Polarized Raman spectra along [001] of a crystal lying in the *ab* plane (Fig. 6) and in the *bc* plane (Fig. 7) reveal several features. Here, we focus on the OH and H_2O bands to localize the proton within the OH group. To a lesser extent, we also consider the main Si—O stretching band. The band observed as a shoulder at approximately 3620 cm ^{1} in the $Z(XX)\overline{Z}$ polarization in Fig. 6, and as a more distinct band at 3626 cm ^{1} in the $X(ZZ)\overline{X}$ polarization in Fig. 7, is attributed to the O—H stretching of the silanol group. The high vibrational frequency supports the absence of hydrogen bonding involving this OH group, in agreement with the findings of Bonaccorsi et al. The opposite case would result in a significant lowering of the O—H stretching vibration due to the weakening of the O—H covalent bond [52]. The polarized Raman spectra further reveal that the (Si)O-H bond lies in the plane perpendicular to the *b*-axis, as shown by its presence only in polarizations within the *a(cosγ)c* plane, and that it has a stronger component along the *c*-axis, as indicated by the enhanced intensity of the 3626 cm ^{1} band in the $X(ZZ)\overline{X}$ polarization. The distribution of hydrogen bonds involving non-protonated (Si)O$_{nbr}$ and H_2O molecules, as described by Bonaccorsi et al., is also confirmed (dotted lines in Fig. 8), predominantly preserving the *b* direction. Fig. 8, which shows the structure of 14 Å tobermorite in different orientations corresponding to the polarization directions, helps to visualize these observations. Biagioni et al. [53], report the Raman spectrum of plombierite (natural analogon of 14 Å tobermorite) observing three bands in the 900–1060 cm ^{1} range: 996 cm ^{1}, 1025 cm ^{1} and 1057 cm ^{1} and assigning them to symmetrical stretching (ν_1-Si-O) of Q.^{2} It should be noted that their spectrum is of low signal-to-noise quality, thus allowing precise determination only of the position of the strongest band at 996 cm ^{1}. Nevertheless, the positions of the remaining two bands are well determined considering our data where the bands are clearly seen at 1031 and 1058–1060 cm ^{1}. Both, Biagioni et al. and our data contrast with the findings reported in [30], where the main band is reported at 1005 cm ^{1}. Another significant discrepancy is the position of the symmetrical Si-O-Si bending mode, reported at 675 cm ^{1} in [30] whereas it appears at 665–666 cm ^{1} (Figs. 6 and 7), as well as in [53]. This raises serious concerns about the quality of the 14 Å tobermorite sample used in [11] and [30].

In our Raman spectra, the symmetrical stretching of ν_1-Si-O$_{nbr}$ is positioned at 998–999 cm ^{1} as it is polarized having the maximal intensity in orientation perpendicular to *b*-axis. Being the most intense stretching band, it is in accordance with findings in [54]. The bands with lower intensity at 1031 and 1058–1060 cm ^{1} could be assigned to ν_1-Si$_{br}$-O.

It is interesting to note that 11 Å tobermorite exhibits very similar polarization behavior in both the Si—O and OH vibrational bands, albeit with slightly different frequencies. These findings will be the subject of a separate manuscript.

3.4.3. Jennite: $Ca_9[Si_3O_9]_2(OH)_6{\cdot}8H_2O$

3.4.3.1. IR polarization spectroscopy. The structure of jennite, $Ca_9[Si_3O_9]_2(OH)_6.8H_2O$, was solved by Bonaccorsi et al. using the Taylor's basic module, known as the tilleyite ribbon [55]. Similar modules are present not only in the name giving structure but also in jaffeite and cuspidine. Unlike 14 Å tobermorite, jennite lacks Si-OH environments of the bridging tetrahedron. Instead, the apical non-bridging oxygen of the bridging tetrahedron, which points to the interlayer, is involved in a double hydrogen bond (O—H = 1.52–1.54 Å). Using first-principles molecular dynamics, Churakov [56] successfully proposed the H positions in the structure, thus allowing to reproduce the hydrogen bonding scheme. Vidmer et al. [12] optimized the jennite structure proposed by Churakov and extensively calculated the density of states (DOS) and vibrational frequencies [12]. Based on these calculations, they made corresponding assignments of bands in the observed spectra. In general, similarly to 14 Å tobermorite, the triple chain of

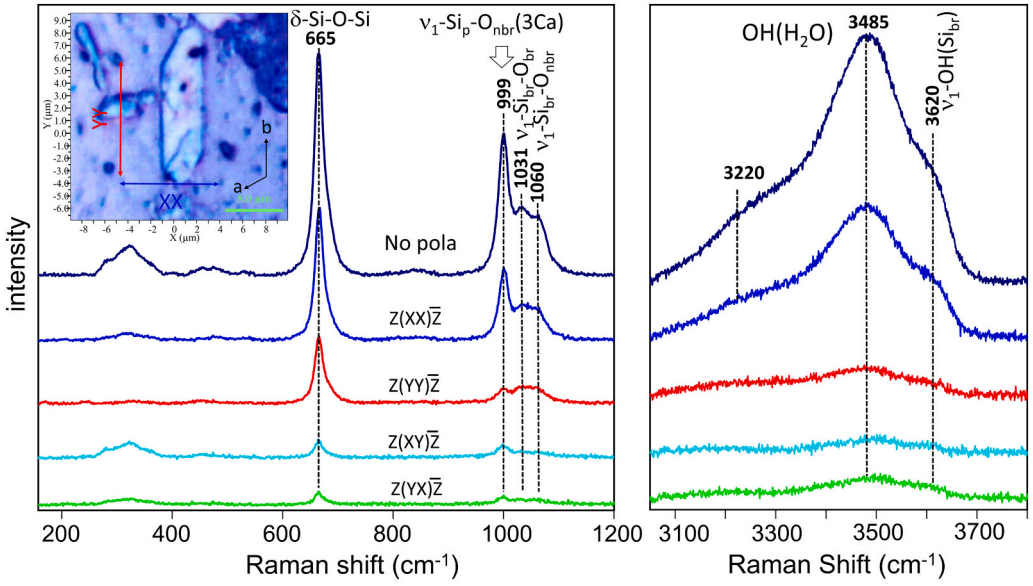

Fig. 6. Polarized Raman spectra of 14 Å tobermorite along ZZ direction. The shoulder of the OH band at 3620 cm^{-1} is seen in the $Z(XX)\overline{Z}$ polarization. In the same direction, an enhanced OH vibration in the H_2O species is also observed.

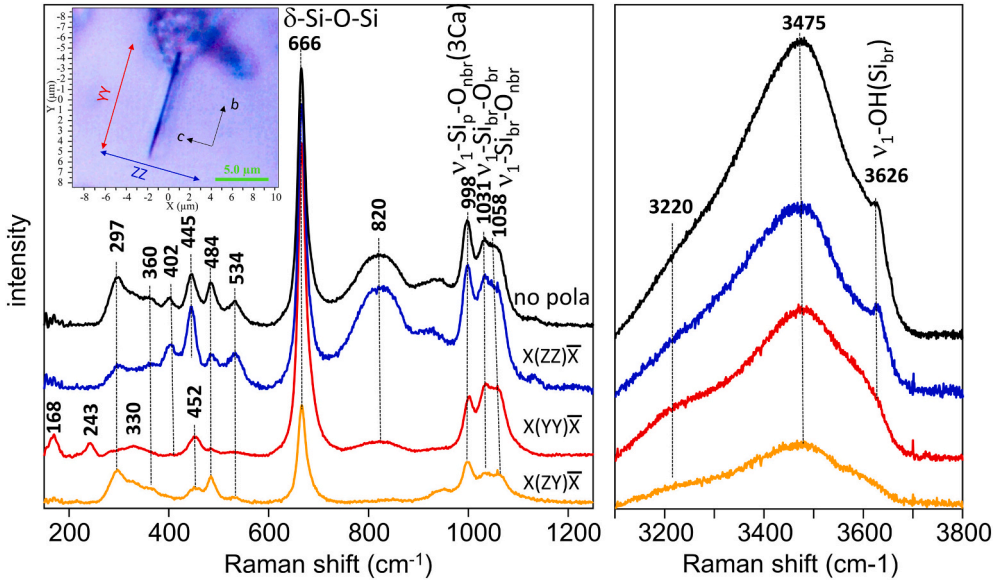

Fig. 7. Polarized Raman spectra of 14 Å tobermorite along XX *(a.cosγ)* direction. The OH band at 3626 cm^{-1} is seen in the $X(ZZ)\overline{X}$ polarization. In $X(YY)\overline{X}$ polarization, the intensity of the band at 3220 cm^{-1} corresponds to stronger H bonding along *b*-axis.

jennite consists of paired tetrahedra connected with a bridging tetrahedron in an infinite chain ("dreiereinfachkette"). While the Si-O-Si angles between both paired and paired-bridging tetrahedra in 14 Å tobermorite are around 138°, those in jennite differ, being 145° between Si_p-O-Si_p tetrahedra and 140° in Si_{br}-O-Si_p tetrahedra. The slightly higher Si-O_{br} frequency observed in the spectra of jennite may be attributed to the larger Si-O-Si angle. Similarly to 14 Å tobermorite, the O_{nbr}'s of the paired tetrahedra (O3, O4, O9 and O10 according to [55]) are shared with 3 Ca atoms (Fig. SI6B). One of the two O_{nbr}'s (O1) of the bridging tetrahedron is shared with two Ca atoms (Ca1, Ca3), with additional influence from a hydrogen bond to a H_2O coordinating interstitial Ca (Ca5) (Fig. SI6A, C). The second is involved in two strong hydrogen bonds provided by H_2O molecules coordinating one interstitial Ca (Ca5) and one Ca from the tilleyite ribbon (Ca4). Additionally, a third longer hydrogen bond connects O8 with H_2O coordinating Ca5 (Fig. SI6C). For better understanding, refer to the structural image of jennite provided in the SI file.

Fig. 9 presents the polarized IR spectra of a jennite single crystal oriented along the [001] axis. The elongation of the lath-shaped crystal coincides with the propagation of the single silicate chains, which corresponds to the *b* crystallographic axis (Fig. SI5, supplemental information file). In the spectrum with the electric vector polarized perpendicularly to *b*-axis ($\vec{E}\perp b$), the main band is observed at 995 cm^{-1}. As seen from the structure plot in the corresponding orientation, the main contribution comes from vibrations of Si-O_{nbr}, mostly due to ν_3-Si_p-O_{nbr} of the paired tetrahedra. Two high-frequency shoulders are present at about 1040 cm^{-1} and 1075 cm^{-1}. In polarization along the *b*-axis of the crystal ($\vec{E}\parallel b$), a sharp band at 959 cm^{-1} and a shoulder at 981 cm^{-1} dominate the spectrum. Additionally, a sharp band with lower intensity is seen at 900 cm^{-1}. These bands can be assigned to Si-O_{br}

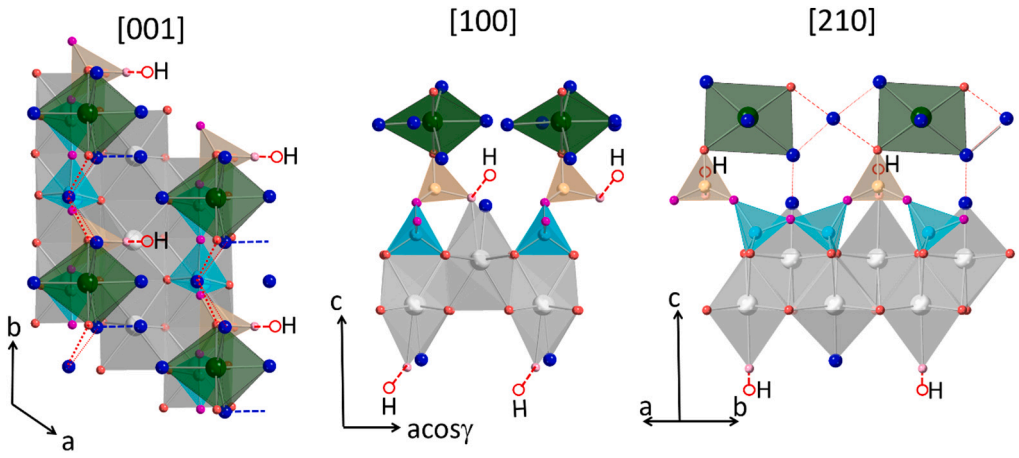

Fig. 8. 14 Å tobermorite structure along [001] (left), [100] (middle), and [210] (right). The strong H-bonds (red dashed lines) between tetrahedron oxygens and H_2O (blue circles) are oriented mostly in the **b** direction, whereas those between H_2O-H_2O (blue dashed lines) are oriented perpendicularly to the **b**-axis. The OH bond lies strictly in the plane a(cosγ)c, with a larger component along the **c**-axis. (For interpretation of the references to color in this figure legend, the reader is referred to the web version of this article.)

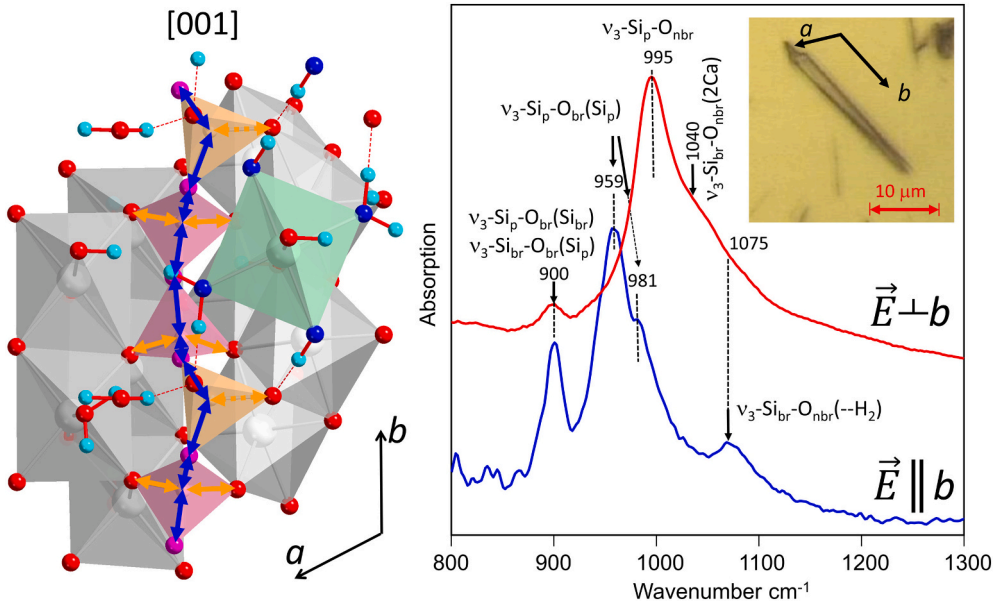

Fig. 9. (Right) Polarized spectra of jennite (acquired with synchrotron light). E∥b-axis (blue), E$^{\perp}$b-axis (red). The assignments correspond to the vibrational directions in the structure with the crystal oriented along the 001 axis. Left: Projection of the structure along [001]. Si-O_{nbr} (orange arrows), SiO_{br} (blue arrows). Paired tetrahedra (pink), bridging tetrahedral (light orange), Ca-polyhedra from the tilleyite slab (grey), interlayer Ca (green), O_{nbr} (red circles), O_{br} (magenta circles), H_2O coordinating interlayer Ca (blue), H (light blue). H positions from [56]. (For interpretation of the references to color in this figure legend, the reader is referred to the web version of this article.)

vibrations, having their largest components in the *b* direction, as indicated by the blue arrows in Fig. 9 (left). The band at 900 cm ^{1} is also seen in the spectrum $\vec{E}^{\perp}b$, albeit with very low intensity. Vidmer et al. [12], assign the band at 900 cm ^{1} to the stretching of Si_p-O_{nbr}, which contradicts the polarized spectra. It should also be noted that the optimized bond length of Si-O [12,56] is about 1.62–1.63 Å for Si-O_{nbr} whereas it is 1.65–1.67 Å for Si-O_{br}. Therefore, it is expected that the vibrating frequency of Si-O_{nbr} is higher. The bands at higher frequencies, 959 cm ^{1} and 995 cm ^{1} (Fig. 9, right), were assigned by [12] to Si_p-O_{nbr} (according to their nomenclature O-$SiCa_x$) and to Si-O_{br} (O—Si_2), respectively, which is in contrast to the polarized spectra.

The band with low intensity at 1075 cm ^{1} in the ($\vec{E}\|b$) spectrum, also seen as a shoulder in the ($\vec{E}^{\perp}b$) orientation, could be assigned to Si_{br}-O_{nbr} (O8) stretching. Vidmer et al. [12], calculated a mode for this vibration at 1120 cm ^{1}, but there is no entry for experimentally observed frequencies in their Table 6. Considering the environment of O8 (involved as acceptor of 3 hydrogen bonds) and the directionality of the Si_{br}-O8 band in this orientation, it seems very feasible to make this assignment. The shoulder at 1040 cm ^{1} could be assigned to the vibration of Si_{br}-O1, having a component only perpendicular to the *b*-axis (dashed arrows in Fig. 9, left).

3.4.3.2. Raman polarization spectroscopy. An examination of the polarized Raman spectra reveals a consistent pattern (Fig. 10). The spectrum taken along $Z(XX)\bar{Z}$ displays a strong band at 993 cm ^{1}, with shoulders at lower frequencies (960, 980 cm ^{1}). Additionally, a well-resolved band appears at 1041 cm ^{1}. The spectrum recorded along $Z(YY)\bar{Z}$ shows a hump where at least three peaks might be contributing at approx. 960, 980 and 990 cm ^{1}. The lower intensity of these bands

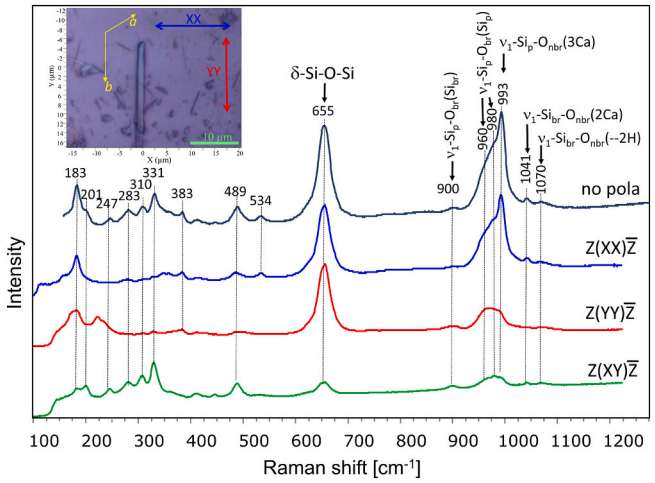

Fig. 10. Polarized Raman spectra of a jennite single crystal (optical microscopic image) taken along the *c*-axis. The elongation coincides with the *b*-axis. The top spectrum is taken without polarizers. The blue spectrum represents polarization perpendicular to the *b*-axis. The red spectrum shows polarization along the *b*-axis. The green spectrum indicates cross polarization (polarized perpendicular to the *b*-axis, analyzed along the *b*-axis). (For interpretation of the references to color in this figure legend, the reader is referred to the web version of this article.)

confirms their association with the stretching vibrations of Si-O_{br}.

Interestingly, the band positions in the Raman spectra correspond quite well with those in the IR spectra, even showing the small band at 1070–1075 cm ^{1}, which is polarized in the IR spectrum. In comparison, the work of [30] presents a rather simplified description of a broad band centered at 970 cm ^{1}, and the authors assign a similar band in their Raman spectrum to CO_3 stretching. While we cannot rule out carbonation in their specimen, in our case, using single crystals, the band is clearly not due to CO_3, especially given its strong polarization. We prefer the assignment of this band to an interaction of the Si-O_{br} with neighboring H_2O molecules, as we proposed in [31]. Although the assignment by Kirkpatrick et al. [30] appears to be questionable, it has been directly adopted in several later studies concerning the Raman spectra of C-S-H and C-A-S-H phases [22,32].

The orientation of the OH groups in jennite and their thermal behavior during the transition to metajenite will be addressed in a separate manuscript due to the complexity of the subject.

3.5. *Summary of the assignment of C-S-H modes*

Summarizing the findings of the polarized IR spectroscopy, we can assign the most intense band at 934 cm ^{1} in the IR spectra of the C-S-H phases (Fig. 2B and Table 1) to ν_3-Si-O_{nbr} in dimers (C/S = 3/2, 4/3). As the C/S ratio decreases, the ν_3-Si-O_{nbr} of chain-like species dominate the spectra, giving rise to the band at 960 cm ^{1}. The low-frequency shoulder at 920 cm ^{1} indicates the formation of Q^2 units and can be assigned to ν_3-Si-O_{br} in the bridging and paired tetrahedra. Similar assignment was given in [32]. However, the authors refer to calculated modes for jennite at 920 cm ^{1} (930 cm ^{1} for 14 Å tobermorite) in the paper of Vidmer et al. [12] who themselves connect this mode with observed frequencies at much higher frequency. The results from polarization IR on 14 Å tobermorite in this work and the calculations of Vidmer et al. [12], justify the assignment of the bands 920–930 cm ^{1} to vibrational modes with participation of the bridging tetrahedra in Yan et al. [32]. The importance of this assignment becomes evident when taking a closer look at the IR spectra of C-A-S-H phases with a C/S ratio of 1 and varying A/S ratios (0–0.2), as presented in [22]. The shoulder on the low-frequency side of the main Si(Al)-O envelope is again correctly attributed to the involvement of bridging tetrahedra. However, in their Table 1, the authors report a frequency of 920 cm ^{1}, although both the spectra and their second derivatives shown in their Fig. 5a clearly indicate a considerably lower frequency, even below 900 cm ^{1}. This discrepancy is understandable, considering that the references cited in their Table 1 pertain to C-S-H rather than C-A-S-H phases. The observed shift of the shoulder to lower frequencies with increasing Al content in bridging sites is attributed to the lower electronegativity of Al (1.6) compared to Si (1.9), resulting in longer Al—O bonds.

The higher frequency band at approximately 1007 cm ^{1} gains intensity in the sample with C/S = 2/3. In contrast to 14 Å tobermorite, the lower Ca content in the interlayer of the C-S-H phases with C/S < 5/6 leads to underbonded O_{nbr} in the bridging tetrahedra. Another difference is the higher number of the silanol groups required to maintain charge balance in the C-S-H structure [57,58]. Nyfeller and Armbruster indicate that the Si-O(H) bond lengths should decrease with increasing silicate polymerization in terms of number of bridging oxygens [59] and therefore the corresponding stretching mode is expected at higher vibrational frequency. However, if silanol groups are additionally involved in H-bonds, these frequencies should be observed at even higher wavenumbers, as shown in [48] and references therein. The disordered nature of the C-S-H phases and especially of the OH-H_2O interactions, not only strongly influences the Si_{br}-O_{nbr} vibrational frequency shifting it to higher wavenumbers, but also leads to the occurrence of the broad band at 1130 cm ^{1}. Therefore, the band at 1007 cm ^{1} can be assigned to the ν_3-Si-O_{nbr} from the bridging tetrahedra. In the middle of the envelope, contributions of the ν_3-Si-O_{br} should be also expected, but beyond the mentioned shoulder at 920 cm ^{1}, they are indistinguishable. Additionally, symmetrical stretching ν_1-Si-O_{br} and Si-O_{nbr} is also allowed, as shown by Raman spectroscopy [31], but due to the small IR cross-section of the symmetrical vibrations, their intensity would be small. It should be noted that the assignment of low-intensity bands on both sides of the main envelope to stretching vibrations in the bridging tetrahedra, as proposed in several studies [22,32], is generally correct. However, the present manuscript offers additional assignment details and direct evidence supporting these interpretations.

The new assignment approach enables a critical reassessment of findings reported in previous studies.

The findings of this work are summarized in Table 1 and compared with corresponding IR and Raman spectroscopic data available in the literature. During this comparison, significant discrepancies were identified. One such case, previously discussed, concerns the data reported by Kirkpatrick et al. [30] on 14 Å tobermorite. These data have influenced subsequent studies, such as that of Vidmer et al. [12], where the authors attempted to align their calculations with the experimental data from [11].

In the already cited study by Yan et al. [22], the authors erroneously assign a band at 840 cm ^{1} in the Raman spectrum of C-S-H with C/S = 1.0 to the Si—O symmetric stretching of Q^1 species (their Table 2). However, they clearly refer to the band between 890 and 900 cm ^{1} (their Fig. 5) which is in accordance with the data reported in [30,31].

In another example, Higl et al. [9] stated that after preprocessing the *in situ* ATR spectra, the main band of C-S-H is positioned at 1005 cm ^{1}, belonging to Q^1. While this assignment is correct, it should be supplemented by adding the mode ν_3-Si-O_{nbr}. However, it is evident that the preprocessing of the data influenced the position of the main band. According to the authors, a band at 1005 cm ^{1} initially grows, assigned to Q^1 (dimeric species), followed by the appearance of a band at 950 cm ^{1}, attributed to more polymerized (Q^2) silicates. This interpretation is inconsistent for two main reasons. First, as clearly shown in the *in situ* spectra of hydrated CEM (Fig. 2A) (and supported by over a hundred similar experiments conducted in our laboratory) the main band at 940 cm ^{1} appears first. Second, the assignment of the bands around 940 cm ^{1} (which is the main band in both synthetic and *in situ* formed C-S-H, appearing in the 930–960 cm ^{1} region) to Q^2 silicate units is incorrect.

This is because: a) it is not possible to distinguish between Q^1 and Q^2 species at the early stages of hydration; b) the silicate species formed at

Table 1
Assignment of IR and Raman bands in the Si—O stretching region of C-S-H and related compounds. Abbreviations: s. strong, vs. very strong, m. moderate, w. weak, sh. shoulder, br. broad band, p. polarized. The Raman frequencies marked as "this study" are modified from [31] based on the findings of the present work.

Phase	IR					Raman				
	This study		Previous			This study		Previous		
	[cm ^{1}]	Mode	[cm ^{1}]	Mode	Ref.	[cm ^{1}]	Mode	[cm ^{1}]	Mode	Ref.
Jaffeite	826 s. p.	δ-O-Si-O + ν_3-SiO_{br})	831	ν_3-Si-O	[48]					
	968 vs. p.	ν_3-Si-O_{nbr}	951							
	980 sh. p.	ν_3-Si-O_{nbr}								
	1049 s.p.	ν_3-Si-O_{br}	1050							
14 Å toberm.	834 w. p.	ν_3-Si_{br}-O_{nbr}(H,Ca)	830	ν_3-Si_{br}-O(H)		665 vs.	δ-Si-O-Si	664 s.	δ-Si-O-Si	[53]
	910 s.	ν_3-Si_p-O_{br}(Si_b)				820 br. p.	ν_1-Si_{br}-O_{nbr}(H,Ca)	850 w	Q^1	[30]
	927 s.	ν_3-Si_p-O_{br}(Si_p)				1000 vs. p.	ν_1-Si_p-O_{nbr}(3Ca)	996 vs.	ν_1-Si-O (Q^2)	
	960 s.	ν_3-Si_{br}-O_{br}				1031 m.	ν_1-Si_{br}-O_{br}	1025 m.	ν_1-Si-O (Q^2)	
	971 s.	ν_3-Si_p-O_{nbr}(3Ca)	969	ν_3-O-SiCax	[11,12]	1060 m.	ν_1-Si_{br}-O_{nbr}	1057 sh.	ν_1-Si-O(H) (Q^2)	
	1035 sh.	ν_3-Si_{br}-O_{nbr}(2Ca)	1050	ν_3-O-SiCa	[11,12]			1005	Q^2	[30]
			1120	ν_3-$O-Si_2$	[11,12]	3626 m. p.	ν_1-OH(Si_{br})	675	δ-Si-O-Si	[30]
			1200	ν_3- Si_2-O(H_2O)				1070	CO_3	[30]
Jennite						655 vs.	δ-Si-O-Si	655	δ-Si-O-Si	[30]
	900 s.	ν_3-Si_p-O_{br}(Si_{br})	902	ν_3-O-SiCax	[11,12]	900 w.	ν_1-Si_p-O_{br}(Si_{br})			
	959 vs. p.	ν_3-Si_p-O_{br}(Si_p)	964	ν_3-O-SiCax	[11,12]	960 m. sh.	ν_1-Si_p-O_{br}(Si_p)	970	ν_1-Si-O	[30]
	981 sh.	ν_3-Si_p-O_{br}(Si_p)	984	ν_3-O-Si2	[11,12]	980 sh.	ν_1-Si_p-O_{br}(Si_p)			
	995 s. p.	ν_3-Si_p-O_{nbr}(3Ca)				993 vs. p.	ν_1-Si_p-O_{nbr}(3Ca)			
	1040 sh.	ν_3-Si_{br}-O_{nbr}(2Ca)				1041 w. p.	ν_1-Si_{br}-O_{nbr}(2Ca)			
	1075 m.	ν_3-Si_{br}-O_{nbr}(–2H)	1081	ν_3-O-Si2		1070 w.	ν_1-Si_{br}-O_{nbr}(–2H)	1077	C-O	[30,32,22]
C-S-H (hcp)	816 s.	δ-O-Si-O + ν_3-SiO_{br})	807	Q^1	[11]					
HPC	840 w.	δ-OH(Ca)	944	Q^2	[11]					
	940 vs.	ν_3-Si-O_{nbr}	1007	Q^1	[9]					
	1015 sh.	ν_3-Si-O(–H)	1059	Q^2	[11,12]					
			1105	Q^2	[11,12]					
C-S-H (sy)	666 m.	δ-Si-O-Si				672 vs.	δ-Si-O-Si	672	δ-Si-O-Si	[32]
C/S = 3/2	807	δ-O-Si-O + ν_3-SiO_{br})	809	Q1	[10]	889 m.	ν_1-Si-O_{nbr}(Q^1)	870–900	ν_1-Si-O(Q^1)	[30,32]
	860 w.	δ-OH(Ca)				1022 s.	ν_1-Si-O_{br}(Q^1)	950–1010	ν_1-Si-O(Q^2)	[30,32]
	934	ν_3-Si-O_{nbr}	946	Q1	[10]		ν_1-Si_{br}-O_{br}(Q^2)			
	1025	ν_3-Si-O(–H)	1080	Q1	[10]		ν_1-Si_p-O_{nbr}(Q^2)			
C-S-H (sy)	666 m.	δ-Si-O-Si	670	δ-Si-O-Si		670 vs.	δ-Si-O-Si	670	δ-Si-O-Si	[32]
C/S = 1.0	805	δ-O-Si-O (+ν_3-SiO_{br})	810	Si-O Q^1	[32]	882 w.	ν_1-Si-O_{nbr}(Q^1)	882	ν_1-Si-O(Q^1)	[32]
	860 w.	δ-OH(Ca)				1017 s.	ν_1-Si_{br}-O_{br}(Q^2)	1020	ν_1-Si-O(Q^2)	[32]
	955 vs.	ν_3-Si-O_{nbr}	960	Si-O stretch			ν_1-Si_p-O_{nbr}(Q^2)			
	1007 sh.	ν_3-Si_{br}-O_{nbr}(H)					ν_1-Si-O_{br}(Q^1)			
	1050 sh.	ν_3-Si-O(–H)	1050	Si-O Q^2						
	1130 sh.	ν_3-Si_{br}-O_{nbr}(–H)								
C-S-H (sy)	668 m.	δ-Si-O-Si	670			668 vs.	δ-Si-O-Si			
C/S = 2/3	839 w.	ν_3-Si_{br}-O_{nbr}(H,Ca)	836	Q2	[10]	882 w.	ν_1-Si-O_{nbr}(Q^1)			
	920 sh.	ν_3-Si-O_{br}(Q^2)				1012 s.	ν_1-Si_{br}-O_{br}			
	960 vs.	ν_3-Si_p-O_{nbr}	962	Q2	[10]		ν_1-Si_p-O_{nbr}(3Ca) (Q^2)			
	1007 s.	ν_3-Si_{br}-O_{nbr}(H)				1040 sh.	ν_1-Si_{br}-O_{nbr}(H)			
	1050 sh.	ν_3-Si-O(–H)					ν_1-Si_{br}-O_{nbr}(–2H)			
	1130 sh.	ν_3-Si_{br}-O_{nbr}(–H)	1110	Q2	[10]					

these early stages are mostly dimeric; and c) all dimeric crystalline C-S-H phases (Q^1) exhibit their most intense bands in the 950–980 cm ^{1} range (see Fig. 3). Furthermore, the trend toward polymerization is the opposite of what is suggested. With increasing polymerization, the ν_3-Si-O_{nbr} mode of chains vibrates at a higher frequency than that of dimers, shifting from 934 cm ^{1} to 960 cm ^{1} as seen from Fig. 2B. The oversimplified interpretation of IR bands as being clearly divisible into Q^1 and Q^2 species is widespread in the literature, where the band around 800 cm ^{1} is often assigned to Q^1 and those around 940–960 cm ^{1} to more polymerized species. However, the present work demonstrates that the main IR band in the spectra of all C-S-H phases arises from the stretching of Si-O_{nbr} bonds, regardless of whether they belong to dimers or longer chain silicate species. In the case of dimers, the overpopulation of Si–O_{nbr} bonds (O_{nbr}/O_{br} = 6:1) is the determining factor contributing to their intensity. For longer species, up to single chains (O_{nbr}/O_{br} = 1), the confinement of the Si-O_{br}-Si vibration along the chain propagation once again enhances the intensity of the Si-O_{nbr} vibrations.

This fact highlights once more the similarity of the polymerized C-S-H with 14 Å tobermorite.

The observed shift of the IR band from 1025 to 1007 cm ^{1} with decreasing Ca content of the synthetic C-S-H phases can be compared with the effect of lowering the Si—O stretching frequency upon decreasing the quantity or the field strength of cations, as observed in glasses by [60] and references therein.

As already mentioned in chapter Band assignment of the C-S-H phases: general remarks with reference to literature data, Ylmen et al. [8] give very limited information about assignment of the C-S-H bands. Their claim that a band at 1350 cm ^{1} should be assigned to combination of Si—O stretching and Si-OH bending seems inexplicable. The overall increase of the area of the C-S-H bands with the progress of the hydration is not taken into account. Considering the discussion about the influence of particle size and available space for growth and maturing of the hydrates it is expected (and observed) that the IR bands undergo evolution, which should be considered upon evaluation. Additionally, in this case the preprocessing of the spectra also seems to have negatively influenced the results, leading to inconsistencies with other data.

4. Conclusions

In this work, the main features in the high-frequency envelope of the Si—O stretching range in the IR spectra of C-S-H phases were systematically investigated. For the very first time, IR polarized spectra of

jaffeite, and IR and Raman polarized spectra of 14 Å tobermorite and jennite are presented. The direct observation of the polarization behavior of vibrational modes allowed unambiguous assignment of the bands. In the case of 14 Å tobermorite, the polarized Raman spectra were used to assign the direction of the OH band, which seems to be perpendicular to the *b*-axis with a larger component in the *c* direction. The Si—O stretching vibrations were successfully fragmented into Si_p-O_{nbr}, Si_p-O_{br}, Si_{br}-O_{br}, Si_{br}-O_{nbr}, Si_{br}-OH, and Si_{br}-O(H-bonds) modes where relevant. These assignments were compared to existing data, mostly from theoretical calculations. It has been shown that the main band in the Si—O region is due to Si_p-O_{nbr} stretching vibrations, which possess higher frequency and intensity compared to Si-O_{br} vibrations due to their shorter bond lengths and greater abundance in dimeric species. In the chain silicates 14 Å tobermorite and jennite, the predominant band is due to Si_p-O_{nbr} vibrations, owing to their relatively uniform Ca environment on one side. On the other side, the Si-O_{br} stretching vibrations seem to be naturally constrained along the chain direction and are further characterized by greater variability in Si-O_{br} bond lengths and Si-O-Si angles. Therefore, our analysis of the crystalline phases leads to the general conclusion that Si-O_{nbr} vibrations in the silicate stretching region dominate bulk spectra of both C-S-H phases and crystalline calcium silicate hydrates. The presence, frequency and intensity of the satellite bands (below 900 cm ^{1} and in the range 1000–1200 cm ^{1}) seem to be strongly influenced by the environments of the O_{nbr} belonging to the bridging tetrahedra of triple chain calcium silicate hydrates. These environments vary in terms of presence and number of Ca atoms, OH groups and H-bonds with H_2O molecules in the interlayer.

Although frequently used, frequency alone may not be a sufficient criterion for determining the length of silicate species, given the complex chemistry of the cement systems. The main vibration in the spectra of the C-S-H phases indeed shifts to higher frequency with an increasing population of the bridging tetrahedra, but there is only a moderate change of 20–25 cm ^{1} in the whole range from pure dimeric to chain silicate units.

Other spectral features, like the intensity of the pure Q^1 band at 805–820 cm ^{1}, or the presence of side bands and shoulder around the main envelope characteristic of vibrations involving bridging Si as Si-O_{nbr}, Si-O_{nbr}(H) or Si-O_{nbr}(-H-O-H) should be considered too.

The nature of the IR band in the range of 800–830 cm ^{1}, present in the spectra of Ca-rich C-S-H phases and their crystalline dimeric counterparts, was elucidated. It seems to be due to the simultaneous movement of all seven oxygens parallel to the Si—Si direction of the dimer. As it is present in all Si_2O_7 structures irrespective of the nature of the cations, this finding has universal significance.

The vibrational modes in the spectra of the synthetic C-S-H phases were reassigned, considering both the data on silicate speciation from ^{29}Si NMR and TMS, and the findings from the polarized spectra of the crystalline compounds. The resemblance of the IR spectra of both synthetic C-S-H and those formed upon hydration of CEM I eliminates some uncertainties observed in *in situ* IR experiments so far. Thus, a solid basis for the correct interpretation of *in situ* IR spectra of cement hydration is provided.

CRediT authorship contribution statement

Krassimir Garbev: Writing – review & editing, Writing – original draft, Visualization, Methodology, Investigation, Formal analysis, Data curation, Conceptualization. **Biliana Gasharova:** Writing – review & editing, Methodology, Investigation, Formal analysis. **Angela Ullrich:** Writing – review & editing, Investigation, Formal analysis, Data curation. **Günter Beuchle:** Writing – review & editing, Visualization, Methodology, Investigation, Formal analysis. **Peter Stemmermann:** Writing – review & editing, Methodology, Investigation.

Declaration of competing interest

The authors declare that they have no known competing financial interests or personal relationships that could have appeared to influence the work reported in this paper.

Acknowledgments

We thank Dr. Michael Fechtelkord at Geoscience NMR "Geowissenschaftliches NMR Spektrometer", Institute of Geology, Mineralogy and Geophysics, Ruhr-Universität Bochum, Dr. Olivia Wenzel (KIT, LEM) for TEM measurements, Dr. Siegfried Kreisz, Julia Podszuweit (KIT-ITC) for TMS experiments.

We acknowledge the KIT light source for provision of instruments at the IR2 beamline and we would like to thank the Institute for Beam Physics and Technology (IBPT) for the operation of the storage ring, the Karlsruhe Research Accelerator (KARA). We also thank Dr. Yves-Laurent Mathis for assistance in using beamline IR2.

Data availability

Data will be made available on request.

References

[1] E. John, B. Lothenbach, Cement hydration mechanisms through time – a review, J. Mater. Sci. 58 (2023) 9805–9833, https://doi.org/10.1007/s10853-023-08651-9.

[2] K.L. Scrivener, T. Matschei, F. Georget, P. Juilland, A. Kunhi Mohamed, Advances in hydration and thermodynamics of cementitious systems, Cem. Concr. Res. 174 (2023) 107332, https://doi.org/10.1016/j.cemconres.2023.107332.

[3] Y. Yue, J.J. Wang, P.A. Muhammed Basheer, Y. Bai, In-situ monitoring of early hydration of clinker and Portland cement with optical fiber excitation Raman spectroscopy, Cem. Concr. Compos. 112 (2020) 103664, https://doi.org/10.1016/j.cemconcomp.2020.103664.

[4] J. Kalkreuth, A. Ullrich, K. Garbev, D. Merz, P. Stemmermann, D. Stapf, Accelerated carbonation of hardened cement paste: quantification of calcium carbonate via ATR infrared spectroscopy, J. Am. Ceram. Soc. 107 (4) (2023) 2627–2640, https://doi.org/10.1111/jace.19546.

[5] V.H.J. Mendes dos Santos, D. Pontin, G.G.D. Ponzi, A.S. de Guimarães e Stepanha, R.B. Martel, M.K. Schütz, S.M.O. Einloft, F. Dalla Vecchia, Application of Fourier transform infrared spectroscopy (FTIR) coupled with multivariate regression for calcium carbonate ($CaCO_3$) quantification in cement, Constr. Build. Mater. 313 (2021) 125413, https://doi.org/10.1016/j.conbuildmat.2021.125413.

[6] H.F.W. Taylor, Hydrated calcium silicates part I compound formation at ordinary temperatures, J. Chem. Soc. (1950) 3682–3690.

[7] D.L. Kantro, S. Brunauer, C.H. Weise, Development of surface in the hydration of of calcium silicates II. Extension of investigations to earlier and later stages of hydration, J. Phys. Chem. 66 (10) (1962) 1804–1809, https://doi.org/10.1021/j100816a007.

[8] R. Ylmén, U. Jäglid, I. Panas, Monitoring earqaly hydration of cement by ex situ and in situ ATR-FTIR - a comparative study, J. Am. Ceram. Soc. 97 (2014) 3669–3675, https://doi.org/10.1111/jace.13186.

[9] J. Higl, D. Hinder, C. Rathgeber, B. Ramming, M. Lindèn, Detailed in situ ATR-FTIR spectroscopy study of the early stages of C-S-H formation during hydration of monoclinic C_3S, Cem. Concr. Res. 142 (2021) 106367, https://doi.org/10.1016/j.cemconres.2021.106367.

[10] E. John, D. Stephan, Calcium silicate hydrate - in-situ development of the silicate structure followed by infrared spectroscopy, J. Am. Ceram. Soc. 104 (2021) 6611–6624, https://doi.org/10.1111/jace.18019.

[11] P. Yu, R.J. Kirkpatrick, B. Poe, P.F. McMillan, X.D. Cong, Structure of calcium silicate hydrate (C–S–H): near-, mid-, and far-infrared spectroscopy, J. Am. Ceram. Soc. 82 (3) (1999) 742–748, https://doi.org/10.1111/j.1151-2916.1999.tb01826.x.

[12] A. Vidmer, G. Sclauzero, A. Pasquarello, Infrared spectra of jennite and tobermorite from first-principles, Cem. Concr. Res. 60 (2014) 11–23, https://doi.org/10.1016/j.cemconres.2014.03.004.

[13] D. Massiot, F. Fayon, M. Capron, I. King, S. Le Calvé, B. Alonso, J.-O. Durand, B. Bujoli, Z. Gan, G. Hoatson, Modelling one- and two-dimensional Solid State NMR spectra, Magn. Reson. Chem. 40 (2002) 70–76, https://doi.org/10.1002/mrc.984.

[14] D. Hoebbel, G. Garzo, G. Engelhardt, A. Vargha, Über die Konstitution und Verteilung der Silicatanionen in wässrigen Tetramethylammonium-

Silicatlösungen, Z. Anorg. Allg. Chem. 494 (1) (1982) 31–42, https://doi.org/10.1002/zaac.19824940104.
[15] E. Tajuelo Rodriguez, I.G. Richardson, L. Black, E. Boehm-Courjault, A. Nonat, J. Skibsted, Composition, silicate anion structure and morphology of calcium silicate hydrates (C-S-H) synthesised by silica-lime reaction and by controlled hydration of tricalcium silicate (C_3S), Adv. Appl. Ceram. 114 (7) (2015) 362–371, https://doi.org/10.1179/1743676115Y.0000000038.
[16] L. Black, K. Garbev, G. Beuchle, P. Stemmermann, D. Schild, X-ray photoelectron spectroscopic investigation of nanocrystalline calcium silicate hydrates synthesised by reactive milling, Cem. Concr. Res. 36 (2006) 1023–1031, https://doi.org/10.1016/j.cemconres.2006.03.018.
[17] S. Dent-Glasser, E.E. Lachowski, M.Y. Qureshi, H.P. Calhoun, D.J. Embree, W. D. Jamieson, C.R. Masson, Identification of some of the polysilicate components of trimethylsilylated cement, Cem. Concr. Res. 11 (1981) 775–780, https://doi.org/10.1016/0008-8846(81)90036-3.
[18] A.R. Brough, C.M. Dobson, I.G. Richardson, G.W. Groves, In situ solid-state NMR studies of Ca_3SiO_5: hydration at room temperature using ^{29}Si enrichment, J. Mater. Sci. 29 (1994) 3926, https://doi.org/10.1007/BF00355951.
[19] I.G. Richardson, Tobermorite/jennite- and tobermorite/calcium hydroxide-based models for the structure of C-S-H: applicability to hardened pastes of tricalcium silicate, beta-dicalcium silicate, Portland cement, and blends of Portland cement with blast-fumace slag, metakaolin, or silica fume, Cem. Concr. Res. 34 (2004) 1733–1777, https://doi.org/10.1016/j.cemconres.2004.05.034.
[20] A. Baldermann, C. Baldermann, O. Furat, M. Krüger, M. Nachtnebel, H. Schroettner, J. Juhart, V. Schmidt, J. Tritthart, Mineralogical and microstructural response of hydrated cement blends to leaching, Constr. Build. Mater. 229 (2019) 116902, https://doi.org/10.1016/j.conbuildmat.2019.116902.
[21] A. Baldermann, V. Preissegger, S. Imić, I. Letofsky-Papst, F. Mittermayr, M. Dietzel, Uptake of aqueous heavy metal ions (Co^{2+}, Cu^{2+} and Zn^{2+}) by calcium-aluminium-silicate-hydrate gels, Cement Sci. Concr. Technol. 147 (2021) 106521, https://doi.org/10.1016/j.cemconres.2021.106521.
[22] Y. Yan, B. Ma, G.D. Miron, D.A. Kulik, K. Scrivener, B. Lothenbach, Al uptake in calcium silicate hydrate and the effect of alkali hydroxide, Cem. Concr. Res. 162 (2022) 106957, https://doi.org/10.1016/j.cemconres.2022.106957.
[23] A. Priyanka, N.C. Bhat, N.C. Debnath, Theoretical and experimental study of structures and properties of cement paste: the nanostructural aspects of C–S–H, J. Phys. Chem. Solids 72 (8) (2011) 920–933, https://doi.org/10.1016/j.jpcs.2011.05.001.
[24] A. Nonat, The structure and stoichiometry of C-S-H, Cem. Concr. Res. 34 (2004) 1521–1528, https://doi.org/10.1016/j.cemconres.2004.04.035.
[25] S. Garault-Gauffinet, A. Nonat, Experimental investigation of calcium silicate hydrate (C-S-H) nucleation, J. Cryst. Growth 200 (1999) 565–574, https://doi.org/10.1016/S0022-0248(99)00051-2.
[26] E.M. Gartner, A proposed mechanism for the growth of C-S-H during the hydration of tricalcium silicate, Cem. Concr. Res. 27 (5) (1997) 665–672, https://doi.org/10.1016/S0008-8846(97)00049-5.
[27] H.M. Jennings, A model for the microstructure of calcium silicate hydrate in cement paste, Cem. Concr. Res. 30 (2000) 101–116, https://doi.org/10.1016/S0008-8846(99)00209-4.
[28] I.G. Richardson, The nature of C-S-H in hardened cements, Cem. Concr. Res. 29 (1999) 1131–1147, https://doi.org/10.1016/S0008-8846(99)00168-4.
[29] Yu.D. Glinka, M. Jaronec, Shape-selective Raman scattering from surface phonon modesin aggregates of amorphous SiO_2 nanoparticles, J. Appl. Phys. 82 (7) (1997) 3499–3507, https://doi.org/10.1063/1.365667.
[30] R.J. Kirkpatrick, J.L. Yarger, P.F. McMillan, P. Yu, X.D. Cong, Raman spectroscopy of C–S–H, tobermorite, and jennite, Adv. Cem. Based Mater. 5 (1997) 93–99, https://doi.org/10.1016/S1065-7355(97)00001-1.
[31] K. Garbev, P. Stemmermann, L. Black, C. Breen, J. Yarwood, B. Gasharova, Structural features of C–S–H (I) and its carbonation in air—a raman spectroscopic study. Part I: fresh phases, J. Am. Ceram. Soc. 90 (3) (2007) 900–907, https://doi.org/10.1111/j.1551-2916.2006.01428.x.
[32] Y. Yan, S.-Yu Yang, G.D. Miron, I.E. Collings, E. L'Hôpital, J. Skibsted, F. Winnefeld, K. Scrivener, B. Lothenbach, Effect of alkali hydroxide on calcium silicate hydrate (C-S-H), Cem. Concr. Res. 151 (2022) 106636, https://doi.org/10.1016/j.cemconres.2021.106636.
[33] E. Gartner, I. Maruyama, J. Chen, A new model for the C-S-H phase formed during the hydration of Portland cements, Cem. Concr. Res. 97 (Supplement C) (2017) 95–106, https://doi.org/10.1016/j.cemconres.2017.03.001.
[34] A.N. Lazarev, Vibrational Spectra and Structure of Silicates, Consultants Bureau, New York, 1972, pp. 66–72.
[35] E. Dowty, Fully automated microcomputer calculation of vibrational spectra, Phys. Chem. Miner. 14 (1987) 67–79, https://doi.org/10.1007/BF0031115.
[36] E. Dowty, Vibrational interactions of tetrahedra in silicate glasses and crystals, Phys. Chem. Miner. 14 (1987) 122–138, https://doi.org/10.1007/BF00308216.
[37] E. Dowty, Vibrational interactions of tetrahedra in silicate glasses and crystals, Phys. Chem. Miner. 14 (1987) 542–552, https://doi.org/10.1007/BF00308290.
[38] R. Shuker, R.W. Gammon, Raman-scattering selection-rule breaking and the density of states in amorphous materials, Phys. Rev. Lett. 25 (4) (1970) 222–225, https://doi.org/10.1103/PhysRevLett.25.222.
[39] F.L. Galeneer, C. Mikkelsen, Vibrational dynamics in ^{18}O-substituted vitreous SiO_2, Phys. Rev. B 23 (10) (1981) 5527–5530, https://doi.org/10.1103/PhysRevB.23.5527.
[40] I.G. Richardson, The calcium silicate hydrates, Cem. Concr. Res. 38 (2) (2008) 137–158, https://doi.org/10.1016/j.cemconres.2007.11.005.
[41] E. Bonaccorsi, S. Merlino, A.R. Kampf, The crystal structure of tobermorite 14 Å (Plombierite), a C–S–H phase, J. Am. Ceram. Soc. 88 (2005) 505–512, https://doi.org/10.1111/j.1551-2916.2005.00116.x.
[42] J.E. Del Bene, K. Runge, R.J. Bartlett, A quantum chemical mechanism for the water-initiated decomposition of silica, Comput. Mater. Sci. 27 (1–2) (2003) 102–108, https://doi.org/10.1016/S0927-0256(02)00432-9.
[43] S. Saburi, A. Kawahara, C. Henmi, I. Kusachi, K. Kihara, The refinement of the crystal structure of cuspidine, Min. J. 8 (5) (1977) 286–298, https://doi.org/10.2465/minerj.8.286.
[44] T. Armbruster, B. Lazic, I.O. Galuskina, E.V. Galuskin, E. Gnos, K.M. Marzec, V. M. Gazeev, Trabzonite, $Ca_4[Si_3O_9(OH)]OH$: crystal structure, revised formula, new occurrence and relation to killalaite, Min. Mag. 76 (3) (2012) 455–472, https://doi.org/10.1180/minmag.2012.076.3.02.
[45] I. Kusachi, C. Henmi, A. Kawahara, K. Henmi, The structure of Rankinite, Min. J. 8 (1) (1975) 38–47, https://doi.org/10.2465/minerj.8.38.
[46] N.V. Chukanov, On infrared spectra of silicates and aluminosilicates, Zap. Vseross. Miner. Obs. 124 (3) (1995) 80–85 (in Russian).
[47] N. Chukanov, Infrared spectra of mineral species: extended library, in: Springer Geochemistry/Mineralogy, Springer Science+Business Media Dordrecht, 2014, pp. 1–17, https://doi.org/10.1007/978-94-007-7128-4.
[48] Y. Okada, H. Ishida, T. Mitsuda, Thermal decomposition of tricalcium silicate hydrate, J. Amer. Ceram. Soc. 77 (1994) 2277–2282, https://doi.org/10.1111/j.1151-2916.1994.tb04594.x.
[49] N.A. Yamnova, K. Sarp, Y.K. Egorov-Tismenk, D.Y. Pushcharovskii, Crystal structure of jaffeite, locality: metamorphic rocks, Kombat region, Namibia, Cryst. Rep. 38 (1993) 464–467.
[50] J. Hanuza, M. Ptak, M. Mączka, K. Hermanowicz, J. Lorenc, A.A. Kaminskii, Polarized IR and Raman spectra of $Ca_2MgSi_2O_7$, $Ca_2ZnSi_2O_7$ and $Sr_2MgSi_2O_7$ single crystals: temperature-dependent studies of commensurate to incommensurate and incommensurate to normal phase transitions, J. Solid State Chem. 191 (2012) 90–101, https://doi.org/10.1016/j.jssc.2012.02.051.
[51] M. Diaz, C. Pecharroman, F. del Monte, J. Sany, J.E. Iglesias, J.S. Moya, C. Yamagata, S. Mello-Castano, Synthesis, thermal evolution, and luminescence properties of yttrium disilicate host matrix, Chem. Mater. 17 (7) (2005) 1774–1782, https://doi.org/10.1021/cm047957b.
[52] E. Libowitzky, Correlation of O–H stretching frequencies and O–H···O hydrogen bond lengths in minerals, Monatshefte für Chemie / Chemical Monthly 130 (1999) 1047–1059.
[53] C. Biagioni, E. Bonaccorsi, S. Merlino, D. Bersani, New data on the thermal behavior of 14Å tobermorite, Cem. Concr. Res. 49 (2013) 48–54, https://doi.org/10.1016/j.cemconres.2013.03.007.
[54] P. McMillan, Structural studies of silicate glasses and melts—applications and limitations of Raman spectroscopy, Am. Mineral. 69 (1984) 622–644.
[55] E. Bonaccorsi, S. Merlino, H.F.W. Taylor, The crystal structure of jennite, $Ca_9Si_6O_{18}(OH)_6{\cdot}8H_2O$, Cem. Concr. Res. 34 (2004) 1481–1488, https://doi.org/10.1016/j.cemconres.2003.12.033.
[56] S.V. Churakov, Hydrogen bond connectivity in jennite from ab initio simulations, Cem. Concr. Res. 38 (2008) 1359–1364, https://doi.org/10.1016/j.cemconres.2008.08.004.
[57] K. Garbev, M. Bornefeld, G. Beuchle, P. Stemmermann, Cell dimensions and composition of nanocrystalline calcium silicate hydrate solid solutions. Part 2: X-ray and thermogravimetry study, J. Am. Ceram. Soc. 91 (9) (2008) 3015–3023, https://doi.org/10.1111/j.1551-2916.2008.02601.x.
[58] A.K. Mohamed, S.C. Parker, P. Bowen, S. Galmarini, An atomistic building block description of C-S-H - towards a realistic C-S-H model, Cem. Concr. Res. 107 (2018) 221–235, https://doi.org/10.1016/j.cemconres.2018.01.007.
[59] D. Nyfeler, T. Armbruster, Silanol groups in minerals and inorganic compounds, Am. Mineral. 83 (1998) 119–125, https://doi.org/10.2138/am-1998-1-211.
[60] L. Grund Bäck, S. Ali, S. Karlsson, D. Möncke, E.I. Kamitsos, B. Jonson, Mixed alkali/alkaline earth-silicate glasses: physical properties and structure by vibrational spectroscopy, Int. J. Appl. Glas. Sci. 10 (2019) 349–362, https://doi.org/10.1111/ijag.13101.